

**DIREK INK WRITING OF WATERBORNE POLYURETHANE AS A
BIOMEDICAL MATRIX: ASSESSING MECHANICAL PROPERTIES AND
THE PERFORMANCE OF CONTROLLED RELEASE**

by:

MADINEH RASTGOO

Submitted to the Graduate School of Engineering and Natural Sciences

In partial fulfillment of the requirements for the degree of

Master of Science

Sabanci University

July 2023

MADINEH RASTGOO 2023 ©

All Rights Reserved

**DIREK INK WRITING OF WATERBORNE POLYURETHANE AS A
BIOMEDICAL MATRIX: ASSESSING MECHANICAL PROPERTIES AND
THE PERFORMANCE OF CONTROLLED RELEASE**

Madineh Rastgoo

MAT, Master Thesis, 2023

Thesis Supervisor: Prof. Dr. Ozge Akbulut

Keywords: Direct ink writing, Waterborne polyurethane, Three-point bending, Controlled release, Drug release profile, Soft matrix

Abstract

Fabrication of soft and strong matrixes with architecturally anisotropic properties holds crucial significance in soft tissue applications. In this thesis, using direct ink writing (DIW), customized waterborne polyurethane (WPU) matrices with various geometries and dimensions were printed at room temperature. Pristine WPU scaffolds, with adjustable fabrication parameters (e.g., infill density, infill pattern, number of perimeters) exhibited mechanical properties (elastic modulus: 20 – 26 KPa, tensile strength: 1000 – 1450 KPa, flexural modulus: 85 – 98 KPa, and flexural strength: 1350 – 1750 KPa) that match the range for soft tissues.

To achieve controlled and efficient release profiles from these matrixes, two drug molecules, an antioxidant (ascorbic acid; AA) and an antibiotic (tetracycline), were incorporated into the WPU scaffolds. By tailoring the printed WPU designs, drug-loaded WPU matrices demonstrated sustained release profiles, with approximately 50% release for AA and 80% release for tetracycline over a four-day period. These results highlight the high potential of WPU-based drug carriers for medicine applications.

**Biyomedikal Matris Olarak su Bazlı Poliüretanın Doğrudan Mürekkeple
Yazılması: Mekanik Özelliklerin ve Kontrollü Salım Performansının
Değerlendirilmesi**

Madineh Rastgoo

MAT, Yüksek lisans Tezi, 2023

Tez Danışmanı: Prof. Dr. Özge Akbulut

Anahtar Kelimeler: Doğrudan mürekkeple yazma, Su bazlı poliüretan, Üç noktalı bükme, Kontrollü salım, İlaç salım profili, Yumuşak matris

Özet

Mimari olarak anizotropik özelliklere sahip yumuşak ve güçlü matrislerin üretimi yumuşak doku uygulamalarında büyük önem taşımaktadır. Bu tezde, doğrudan mürekkeple yazma (DIW) kullanılarak, çeşitli geometri ve boyutlara sahip özelleştirilmiş su bazlı poliüretan (WPU) matrisler oda sıcaklığında basılmıştır. Ayarlanabilir üretim parametrelerine (örneğin dolgu yoğunluğu, dolgu deseni, perimetre sayısı) sahip bozulmamış WPU iskeleleri, yumuşak doku aralığına uyan mekanik özellikler (elastik modül: 20 - 26 KPa, çekme mukavemeti: 1000 - 1450 KPa, eğilme modülü: 85 - 98 KPa ve eğilme mukavemeti: 1350 - 1750 KPa) sergilemiştir.

Bu matrislerden kontrollü ve verimli salım profilleri elde etmek için, WPU iskelelerine bir antioksidan (askorbik asit; AA) ve bir antibiyotik (tetrasiykin) olmak üzere iki ilaç molekülü dahil edilmiştir. Basılı WPU tasarımlarının uyarlanmasıyla, ilaç yüklü WPU matrisleri, dört günlük bir süre boyunca AA için yaklaşık %50 ve tetrasiykin için %80 salım ile sürekli salım profilleri göstermiştir. Bu sonuçlar, tıp uygulamaları için WPU bazlı ilaç taşıyıcılarının yüksek potansiyelini vurgulamaktadır.

Table of Contents

1. Introduction
 - 1.1. Additive manufacturing; 3D printing techniques of biomaterials
 - 1.2. Materials for direct ink writing
 - 1.2.1. Flexible and elastic materials
 - 1.2.2. Waterborne polyurethane
 - 1.3. Rheological requirements; Viscosity and shear thinning
 - 1.4. Mechanical characterization
 - 1.5. Degradation study
 - 1.6. Drug carrier scaffolds
 - 1.7. Problem statement and objectives
2. Materials and methods
 - 2.1. Materials
 - 2.2. Fourier transform infrared spectroscopy (FTIR)
 - 2.3. Rheological characterization
 - 2.4. DIW of WPU inks
 - 2.5. Thermogravimetric analysis (TGA)
 - 2.6. Degradation and swelling study
 - 2.7. Mechanical characterization
 - 2.8. Drug release study
3. Results and discussions
 - 3.1. Fourier transform infrared spectroscopy (FTIR)
 - 3.2. Rheological characterization
 - 3.3. Thermogravimetric analysis (TGA)
 - 3.4. Degradation and Swelling
 - 3.5. Mechanical properties
 - 3.6. Drug release profile
4. Conclusion and future remarks

List of Figures

Figure 1. Schematic of direct ink writing process in this study	3
Figure 2. (a) DIW process parameters [61], (b) the fusion of two filament layers takes place vertically [62]	8
Figure 3. Chemical structure of (a) ascorbic acid [93], (b) tetracycline [89]	12
Figure 4. (a) Schematic illustration of three-point bending test of printed samples and the printed patterns used for mechanical tests b) aligned rectilinear c) aligned rectilinear with 2 walls d) rectilinear e) grid f) triangular.....	17
Figure 5. Rheological characteristics of the WPU inks with different hard segment contents a) dependence of viscosity to shear rate b) oscillatory rheological measurements of the inks including storage modulus (—) and loss modulus (...) as a function of shear stress, and c) Storage (■) and loss (□) modulus as a function of frequency.....	22
Figure 6. Images of a typical 3D-printed WPU scaffold analyzed in this study...	23
Figure 7. FTIR spectra of a) WPU inks and b) printed meshes.....	23
Figure 8. FTIR spectra of a) drugs and b) drug loaded WPU ink.....	24
Figure 9. Thermogravimetry analysis for WPU mesh with different hard segment contents. Solid and dotted lines indicate TG and the corresponding derivatives of TG (DTG), respectively.....	25
Figure 10. The degradation rate of WPU scaffolds in two media, PBS (dotted lines) and DMEM (solid lines)	27
Figure 11. Degradation rate of WPU2 and WPU2-AA scaffolds in PBS.....	28
Figure 12. Swelling ratio of WPU scaffolds in two media, PBS (dotted lines) and DMEM (solid lines)	29
Figure 13. From top to bottom, deformation behavior of WPU scaffolds (1) before loading and (2) after loading. WPU3 scaffold under tensile test, (a) before loading and (b) during the loading. WPU3 scaffold under 3-point bending test, (a) before loading and (b) during loading.....	31
Figure 14. The stress-strain curves of the printed WPU scaffolds under tensile load (a-c), and the force-deformation diagrams under bending load (d-f)	32
Figure 15. a) Effect of infill pattern on a) tensile properties and b) flexural properties of the ink with 20% hard segment (WPU3)	34

Figure 16. a) UV-vis spectra of AA loaded WPU 20 % infill, b) UV-vis spectra of AA loaded WPU 35 % infill, and c) AA release profiles from WPU mesh in PBS (pH=7.4) at room temperature.....35

Figure 17. a) UV-vis spectra of tetracycline loaded WPU 20 % infill, b) UV-vis spectra of tetracycline loaded WPU 35 % infill, and c) Tetracycline release profiles from WPU mesh in PBS (pH=7.4) at 37°C temperature.....37

List of Tables

Table 1. Mechanical properties of the printed meshes with different hard segment contents33

Chapter 1

1. INTRODUCTION

1.1. Additive manufacturing techniques

Additive manufacturing, also known as 3D printing, has emerged as a novel manufacturing method for creating custom, multilateral, and multilayer prototypes in various disciplines. This technique builds structures and intricate geometries by depositing materials layer by layer. It offers advantages in smart manufacturing, including design freedom, complexity, reduced energy, and material consumption. Compared to traditional subtractive manufacturing methods, 3D printing eliminates the need for time-consuming processes involved in designing and manufacturing specialized tools or mesh screens during product development. 3D printing was developed by Charles Hull after he introduced stereolithography (SLA) in 1986, followed by advances in powder bed fusion, fused deposition modeling (FDM), and inkjet printing. Over time, 3D printing has evolved by incorporating diverse methods, materials, and equipment, leading to a transformation in manufacturing and logistics [1-4].

There are technical differences among 3D printing platforms that require specific ink formulations. In stimulation-triggered processes (e.g., SLA), a trigger is introduced at specific spatial locations, for example, a binding solution or laser beam, to cause the liquid or powder reservoir to solidify. It is necessary to optimize the monomer, cross-linker, and photo-initiator ratios in stereolithographic systems to ensure efficient photopolymerization while optimizing inhibitor concentrations to avoid over-polymerization [5]. The deposition-based method produces 3D structures by directly depositing material at specified locations. Deposition using FDM method involves placing thermoplastic polymers as filaments above their melting temperature and extruding them as filaments that solidify upon cooling. The FDM process involves adjusting the temperature according to the filament, as well as melting filaments at high temperatures, which prevents bioactive agents from being directly incorporated into the scaffold. [3]. Direct ink writing (DIW) is a low-temperature alternative to FDM that uses viscoelastic materials such as hydrogels, solvent-based polymers, and colloidal suspensions to print 3D structures. DIW offers easy integration of multiple materials and low processing temperatures, which makes it suitable for bio-fabrication applications, such as tissue regeneration scaffolds and soft robotics [5-9].

Computer-aided design (CAD) software is used to design parts in AM process. An STL file is typically created by exporting surface features from three-dimensional CAD files.

This file serves as the main input file for an AM fabricator, which slices the surface file into many two-dimensional layers (2D) in a virtual environment. Using those 2D layers, an AM machine creates the necessary toolpath along the X and Y axes for direct manufacturing. A three-dimensional part is then formed by sequentially processing each layer over other [2].

3D printing has revolutionized biomedicine by offering advantages over traditional machining and casting methods. It enables the production of complex and patient-specific structures, promoting the fabrication of intricate anatomical models, personalized implants, and prosthetics. In addition, AM facilitates the incorporation of several materials and bioactive compounds to develop advanced biomaterials for tissue engineering. Engineered tissue models provide valuable preclinical platforms to evaluate new therapeutic approaches, and gain insight into disease mechanisms, drug efficacy, and toxicity [10, 11].

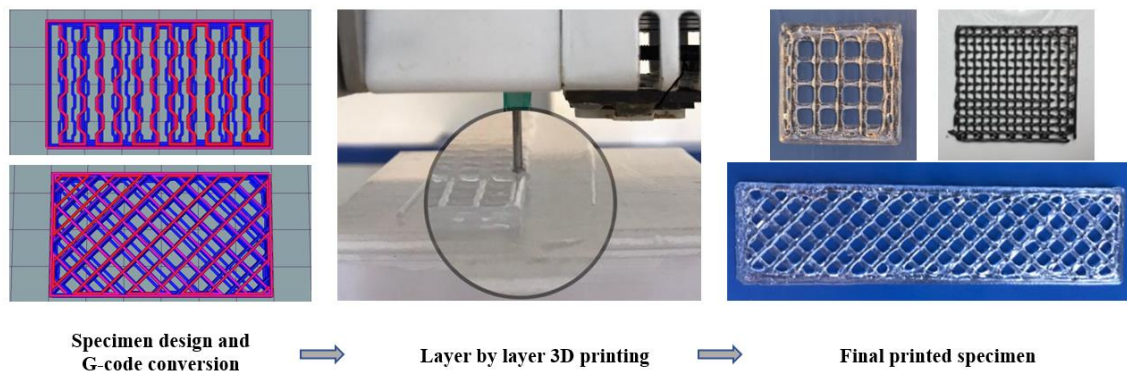


Figure 1. Schematic of DIW process in this study (Axolotl biosystem)

1.2. Materials for DIW

The three main types of inks for DIW are melting, gel-forming, and cold extrusion. Hot melt extrusion inks require heating and cooling to flow and solidify (e.g., polycaprolactone). Gel-forming inks involves chemical or physical crosslinking, often using ions (e.g., alginate and carrageenan) or UV light (e.g., gelatin methacrylate), to create gels. Due to the unsatisfactory mechanical properties of the printed objects, reinforcements have been employed to enhance both printing performance and mechanical properties [12, 13]. Also, UV curing, or a chemical process result in toxic

degradation of products [14]. Cold extrusion inks do not require elevated temperatures during printing and are dependent on ink rheology. The inks must be extruded while forming layers that support themselves. Its rheology is often adjusted by adding additives or thickeners. One significant advantage of cold extrusion inks is that they eliminate additional processing steps such as temperature, crosslinkers, and UV exposure [12].

1.2.1. Flexible and elastic materials

3D matrices or scaffolds can be created using a diverse range of materials, including polymers, ceramics, metals, and composites [6]. In certain applications, such as soft tissue engineering, wound dressing, surgical mesh, sensors, and biorobotics, the inks must possess flexibility and elasticity [16, 21]. In soft tissue engineering, for example, this ensures that the materials can adapt and conform to the surrounding tissues without creating any mismatches between the implants and the tissues. Mechanical discrepancies between scaffolds and host tissues can have detrimental effects. For example, rigid implants placed in soft brain tissue trigger neuroinflammatory responses [15, 16]. Similarly, a mismatch between vascular graft elasticity and native vessel tissue can lead to smooth muscle cell proliferation and vessel occlusion [15, 16]. Tissues naturally endure loads, irrespective of their specific functions, for instance, cartilage tissues can achieve mechanical strength in the megapascal range, while nervous fibers typically exhibit strength in the low kilopascal range [15]. Soft tissues exhibit relatively low elastic modulus, for example heart muscle (20 – 500 MPa), nervous tissues (2 – 200 kPa), and aortic valve (2 – 100 kPa) [16-18]. The Young's Modulus of skin, assessed through indentation tests, typically ranges from 5 to 100 kPa in the thickness-direction, while values of 25 kPa to 140 MPa are commonly observed in tensile and torsion tests [19].

These applications can greatly benefit from synthetic polymers due to their ability to control chemical composition and molecular weight. Synthetic polymers offer a wide range of options for tailoring mechanical properties to meet specific application requirements. [15]. Biocompatible polymers known for their mechanical stability, such as poly-caprolactone (PCL), polylactic acid (PLA), and polylactic-co-glycolic acid (PLGA) have been studied broadly. However, they possess a higher tensile modulus than human soft tissues, which typically ranges from 0.01 to 12 MPa [72]. PCL and PLA engineered scaffolds also have limitations in terms of degradation rates compared to

living tissues. Conversely, PLGA degrades at a faster rate than PCL and PLA, but its bioactivity is constrained due to the acidic degradation products it produces [20, 21]. Polypropylene (PP) is widely employed in mesh implants; however, it exhibits limitations regarding elasticity and strength [22]. Polyurethanes (PUs) possess tunable properties derived from their segmental structure, making them versatile scaffolds capable of exhibiting a wide range of mechanical properties [23]. The strong mechanical properties and low elastic modulus of PUs, which closely resemble soft tissues, make them well-suited for the fabrication of elastic and flexible scaffolds [16]. However, conventional synthetic polymers commonly require the use of organic solvents or elevated temperatures in 3D printing, which can result in toxic effects and prolonged elimination periods, as well as restricted integration of therapeutic agents [24, 25].

1.2.2. Waterborne polyurethane (WPU)

The use of organic solvents in traditional PU presents environmental challenges. To address this, WPU dispersions have emerged as a viable alternative. These dispersions utilize an internal emulsifier that enables the substitution of organic solvents with water, offering benefits such as biodegradability, environmental friendliness, and improved safety. The presence of the internal emulsifier, covalently bonded to the polymer backbone, ensures stability of the particles formed during the phase inversion process. The versatility of WPU is attributed to the variety of reactants that can be combined in their formulation, including polyols, isocyanates, chain extenders, and internal emulsifiers [12, 25-28].

However, in fabrication of matrices that are composed of WPU, challenges arise due to its low viscosity which necessitated the use of composite structures or light-curing procedures in extrusion-based 3D printing. The rheological behavior and printing performance of WPU inks were often modified by the introduction of cellulose derivatives, polyvinyl alcohol, or incorporation of reinforcements (e.g., silica, graphene, silver) [9, 26-31]. Also, freeze drying, and low temperature printing processes have been introduced as a method for WPU scaffold fabrication. Hsieh et al. fabricated a tracheal scaffold using two types of WPU inks through a subzero temperature-printing process as well [32, 33].

1.3. DIW inks rheological properties

To achieve successful DIW printing, it is crucial to evaluate the rheological properties of the ink and the parameters involved in the fabrication process. These factors play a significant role in creating the desired matrix or scaffolds which will be discussed in the following sections. DIW process requires materials that can be extruded through small nozzles and then form shape-stable ink. The rheological properties of materials, which describe how materials deform when under tension, are the most critical physicochemical parameters that influence ink printability. A 3D extrusion-based process changes ink from a bulk to a high-shear condition as it passes through the nozzle. This transition is characterized by viscosity, viscoelastic shear modulus, elastic recovery, and shear stress [1, 6, 34].

1.3.1. Viscosity

Print fidelity is influenced greatly by viscosity, which is the resistance of a fluid to flow under stress; in general, higher viscosities result in higher print fidelity. A polymer's viscosity is controlled primarily by its molecular weight and its concentration. It is known that viscosity is determined by the relationship between shear stress and shear rate; Newtonian fluids are those whose shear stress and shear rate are linearly related, but non-Newtonian fluids are those with a nonlinear relationship. A non-Newtonian fluid may be either time-independent (such as shear-thinning and shear-thickening) or time-dependent (such as thixotropic and rheopectic) [5, 6].

1.3.2. Shear-thinning

Non-Newtonian fluids typically display time-independent shear-thinning behavior, which means they become less viscous with increasing shear rates. Extrusion printing is frequently carried out using materials with this property, such as polymer melts, polymer solutions, hydrogels with partially cross-linked chains, and colloidal suspensions. It is associated with easier extrusion and better initial shape preservation; viscosity decreases during the extrusion phase as shear forces increase. After extrusion, the shear rate falls while the viscosity increases, preserving the printed shape. For time-dependent fluids, ink design does not usually consider the time dependence of the viscosity profile since

adjustment of printing parameters, such as extrusion pressure, would be necessary to maintain a steady flow of ink [5, 6, 12].

1.3.3. Viscoelasticity

Extrusion printing inks exhibit flow and shape retention properties. Inks should flow through nozzles with minimal internal resistance. Once dispensed, however, the properties should be reversed, with a cessation of flow, resistance to deformation, and the ability to retain shape elastically. Viscoelasticity describes the behavior of viscous flow and elastic shape retention, and it is characterized by two parameters, storage modulus (G') and loss modulus (G''). The viscoelastic property can be determined by oscillatory rheology, while viscosity can be assessed by rotation. An oscillation's frequency and amplitude determine G' and G'' respectively [6, 34, 35].

Shear-thinning materials (pseudoplastic) are best suited for DIW. These materials exhibit the advantage of reducing their viscosity as the shear rate increases, making them an ideal material for extrusion processes. During the printing process, the ink viscosity decreases, allowing it to be extruded smoothly through the nozzle at high shear rates. On the other hand, during the steady state with low shear rates, the high viscosity of the ink helps maintain the desired shape of the printed object.

The yield point is a crucial parameter in evaluating material printability in DIW 3D printing. It indicates the stress at which a material's network flows. To successfully extrude the material through the nozzle, the DIW printer must apply a stress higher than the yield point (τ_y). It is also related to the material's ability to maintain its shape under stresses caused by printed layers. The yield point of ink suitable for 3D printing should be low enough to facilitate proper extrusion, but not so low that the printed object spreads out. The yield point is determined by the storage modulus deviating from a constant plateau at low shear stresses. Flow point (τ_f) is also defined as an indicator of when the ink transitions from a solid-like behavior to flowing like a liquid. This is determined by observing the crossover between the storage modulus and the loss modulus [5, 6, 12].

1.4. Fabrication process parameters

DIW printing involves several print parameters that have a significant impact on the quality of the printed structures. These parameters, including layer height (H), print speed

(U_p), extrusion rate I , and nozzle diameter (D), play crucial roles in determining the outcome, Figure 2 (a). The layer height defines the distance between the nozzle and the printing surface. Print speed refers to the velocity at which the printer head moves. The extrusion rate, regulated by the pulse rate of a stepper motor, governs the rate at which the material is extruded through the nozzle. The nozzle diameter, on the other hand, directly influences the printed filament diameter. Ideally, the filament diameter should align with the nozzle diameter. However, factors such as printing speed can lead to filament stretching or ink accumulation, resulting in filament diameter variations. In certain instances, the fusion of adjacent filament layers can cause changes in scaffold height (Δh), Figure 2 (b). The continuity of filament formation is affected by the distance between the needle tip and the substrate, with a larger distance causing ink dripping and disrupting filament formation, while an overly close distance can lead to filament scratching and increased diameter. Furthermore, solvents in DIW printing can shrink the scaffold after drying, potentially affecting its structural and mechanical properties [36, 37].

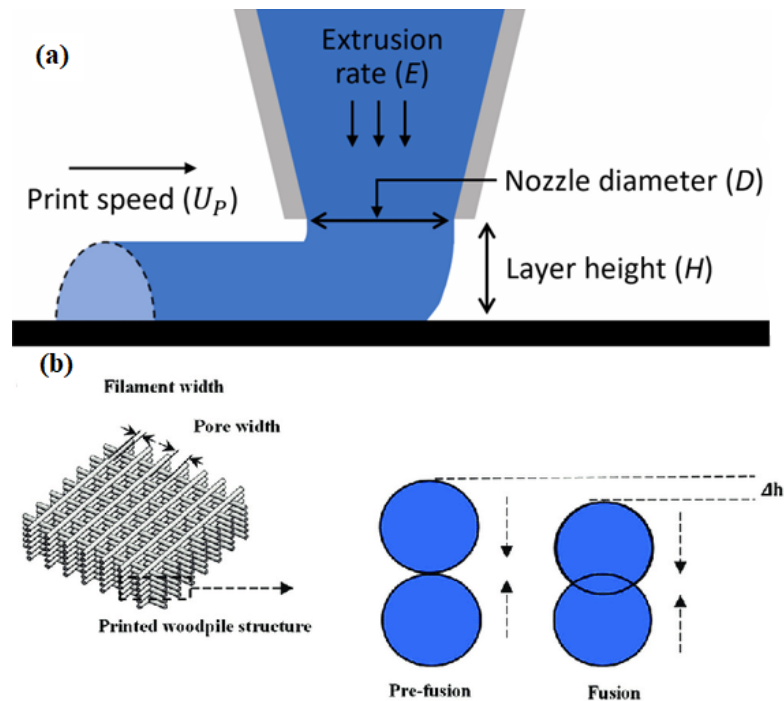


Figure 2. (a) DIW process parameters [36] and (b) the fusion of two filament layers takes place vertically [37].

1.5. Mechanical characterization

Compatibility of the mechanical properties of engineered scaffolds with natural tissues is essential for maintaining structural integrity and stability during implantation. Mimicking the mechanical properties of natural tissues promotes cell attachment, proliferation, and differentiation and enables scaffolds to effectively resemble the mechanical environment of native tissue [1, 10]. Three-point bending test plays a crucial role in characterizing the mechanical performance of scaffolds, contributing to the development of robust and functional structures in tissue engineering [38].

Moreover, mechanical evaluation during degradation is essential for engineered scaffolds. They need to degrade gradually while maintaining structural strength to support tissue healing. For tissue replacement, it is paramount for the mechanical properties of the scaffolds to closely resemble native tissue. Flexural testing is commonly used alongside tensile tests to characterize mechanical properties because it accounts for the various loading modes and potential bending [38].

1.6. Degradation and swelling

Tissue engineering requires scaffolds to degrade at the same rate as the repair process. There are differences in the regeneration mechanisms for each tissue, for example, minimal or no regeneration in the central nervous system and heart, slow cellular renewal in the liver, and active regeneration in the skin and blood [9]. Additionally, scaffold degradation leads to the predictable release of bioactive agents that can reach injured or diseased tissues [35].

Polymers degrade through chemical cleavage of chains, which involves four types of degradation process, including photo, mechanical, thermal, and chemical. The main degradation process after implanting a polymeric scaffold in the body is chemical degradation. Consequently, hydrolytic and enzymatic degradation are the predominant forms of degradation in vivo [39].

Degradation of polymeric scaffold can occur within a few hours (e.g., hydrogel) or over several years (e.g., PCL), which is important to consider based on applications. It is essential that scaffolds provide structural support until cells form their extracellular matrix, without creating toxic products for the cellular environment. Polymers' degradation rates are regulated in several ways: by material composition, media and temperature, surface area, surface treatment, and physical loading. It is important to consider that in vivo scaffolds are subject to a variety of other factors, including enzymes, cellular activity, and pH changes induced by cells, all of which accelerate degradation [9, 40].

Water makes up a substantial percentage of the weight of natural tissues, which makes the swelling capabilities of scaffolds a necessity. Cell adhesion, body fluid absorption, and nutrient diffusion are supported by swelling behavior [37]. In WPU, swelling occurs as liquids are absorbed into the polymer chains without dissolving. This mimics a moist environment, which facilitates healing [41].

1.7. Drug carrier scaffolds

Drug delivery systems improve drug effectiveness by minimizing adverse effects. Conventional methods affect both healthy and unhealthy organs, leading to rapid drug release and necessitating multiple doses, which can increase side effects [42, 43]. Drug delivery systems with controlled release and targeted delivery have become increasingly important, with polymeric scaffolds demonstrating success in controlled release [42]. PUs are used frequently in drug release studies due to their hydrolytic stability, low in vitro protein adsorption, and tunable mechanical properties [44, 45]. Polyurethanes respond to environmental changes (e.g., release media, pH, temperature) by swelling, shrinking, and degrading which enable release of bioagents [46, 47]. By incorporating a microporous architecture, drug carrier scaffolds can enhance their surface area, facilitating drug incorporation and controlled release.

3D printing, specifically extrusion-based printing, offers versatility in creating personalized scaffolds with macro-porous structures, allowing for input materials customization to enable localized drug delivery [22, 43, 48]. This capability is particularly valuable for implantable devices that carry a higher risk of infection. By incorporating antibiotics into the implant, the growth of bacteria on its surface can be prevented, effectively reducing the occurrence of infections [43, 49]. By adjusting the dimensions,

infill pattern, and solid material content of the printed objects, it is possible to produce systems with pre-defined dosages that can be varied as needed [22, 43, 50]. However, heat in FDM processes is essential for accurate printing results as the material needs to solidify after melting. This requirement limits additives such as cells, growth factors, or heat-sensitive drugs during printing. Consequently, FDM in tissue engineering may face significant constraints when incorporating heat-sensitive materials. Conversely, DIW operates in a heat-free environment that involves extruding viscoelastic inks through a nozzle, enabling the incorporation of bioagents without heat or other treatments. This characteristic makes DIW a more suitable choice for integrating heat-sensitive materials into tissue engineering applications [51, 52].

Various medicinal substances are used in tissue engineering and regenerative medicine such as antibiotics, vitamins, growth factors, and anti-inflammatory agents. Among many vitamins, ascorbic acid (vitamin C) is of particular importance due to its anti-inflammatory and antioxidative properties. Lack of L-ascorbic acid inhibits collagen synthesis, angiogenesis, and reduces fibroblast proliferation. Because of impaired host immunity, its deficiency also increases wound infection susceptibility [53, 54].

Tetracycline is a hydrophilic broad-spectrum antibiotic that is widely used in veterinary medicine, human therapy, and as feed additives in the agricultural sector [55, 56]. Tetracycline can promote fibroblast adhesion and is effective against both gram-positive and gram-negative microorganisms by inhibiting bacterial protein synthesis [56, 57]. Loading tetracycline into nanofibers allows for the release of large quantities during wound healing, inhibiting bacterial infection. Bacterial infection during wound healing can impair fibroblast differentiation, compromising normal tissues and the immune system [56]. However, burst release during the initial period may make it challenging to meet long-term antibacterial requirements. Furthermore, achieving long-term release of hydrophilic drugs such as tetracycline from nanofibrous scaffolds is still a challenge due to their high solubility in aqueous mediums [58]. Figure 3 showed the chemical structure of these two drugs as drug model studied in this study.

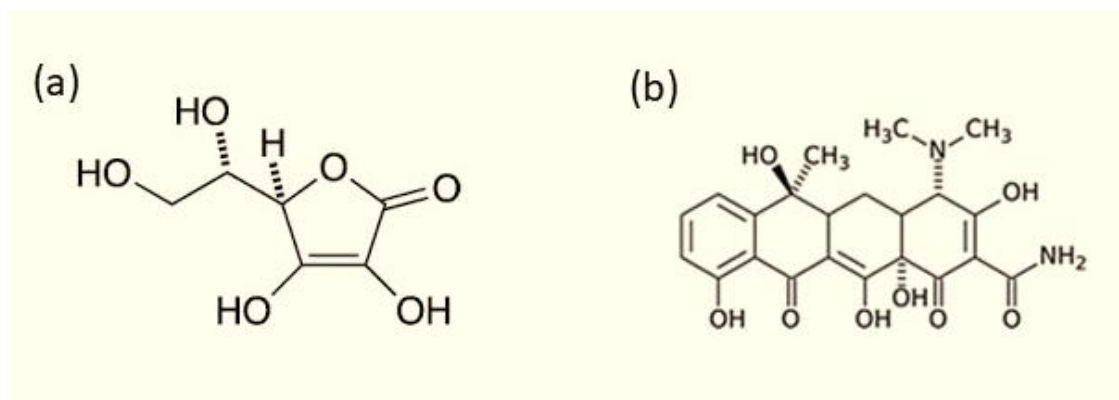


Figure 3. Chemical structure of (a) ascorbic acid [54] and (b) tetracycline [55].

1.8. Motivation and objectives

DIW 3D printing enables the creation of complex 3D designs using viscous liquids, making it an environmentally friendly fabrication method. The ability to fabricate biomedical matrices at ambient temperature through DIW further expands the use of therapeutic agents while preventing thermal degradation and addresses one of the main challenges associated with pharmaceutical formulation extrusion. Moreover, 3D printing offers precise control over scaffold morphology (such as geometry and porosity), which allows tuning mechanical properties and controlling drug release. Conventional synthetic polymers commonly necessitate organic solvents or elevated temperatures in 3D printing, which can result in toxic effects and prolonged elimination periods. Water-based materials, particularly WPU, have gained considerable importance in DIW. WPU offers several advantages over its solvent-based counterparts including biodegradability and eco-friendliness. WPU's mechanical properties can be tailored by adjusting its segmental structure, making it suitable for a wide range of applications. Its water-dispersible structure makes it versatile for delivering bioactive substances and therapeutic agents. WPU dispersions, however, have poor rheological characteristics and exhibit very low viscosities for DIW and need the addition of viscosity modulators.

Therefore, we aim to fabricate WPU structures that mimic mechanical properties of native tissues and intricate architecture without reinforcements or undertaking specific criteria (e.g., heat, UV-light, laser) during printing. A series of WPU inks based on polyol-polyester diisocyanate with different hard segment ratios will be printed through the DIW

process. WPU scaffolds with various patterns will be investigated for their mechanical properties and potential applications. Lastly, the release profile of the two drug models will also be presented using the WPU matrix.

The main objectives are listed as follows:

- Study the rheological behavior of pristine WPU inks.
- Optimize printing parameters including pressure, speed, and feed-rate to achieve desired shape fidelity of a WPU mesh.
- Develop WPU scaffold/matrix with a range of mechanical properties, strength, and modulus, through varying infill percentages and printing patterns.
- Study the release profile of an antibiotic and a vitamin as drug models.

Chapter 2 of the thesis explains the fabrication process of WPU inks, and the design of drug loaded WPU scaffolds. It also outlines the characterization methods utilized throughout the entire process, starting with the inks to the final scaffold. In Chapter 3, the results of the experiments are presented in detail. WPU inks are characterized using FTIR spectroscopy and rheology measurements. Mechanical properties of the printed WPU mesh are studied through three-point bending and tensile tests. TGA analyzes the thermal properties of printed parts. Additionally, UV spectroscopy is employed to obtain the drug release profile from the WPU mesh. The discussion sections include the interpretation of all characterization tests conducted. Finally, Chapter 4 summarizes the overall experimentation process and the results.

Chapter 2

2 . Experimental and methods

2. Materials and Methods

2.1. Materials

WPU inks were synthesized by Dr. Ekin Berksun at SU-IMC, Turkey, phosphate-buffered saline (PBS), Dulbecco's Modified Eagle Medium (DMEM), ascorbic acid, tetracycline.

2.2. FTIR analysis

Fourier transform infrared spectroscopy (FTIR) was utilized to examine the distinctive functional groups present in WPU inks. The measurements were conducted at room temperature, employing a Nicolet IS10 FTIR spectrometer (Thermo Scientific). The analysis spanned from 400 to 4000 cm^{-1} , with a resolution of 2 cm^{-1} , and involved 32 scans.

2.3. Rheological analysis

A comprehensive rheological test was conducted using the Anton-Paar Modular Compact Rheometer (MCR) model 302 rheometer, which featured a gap size of 0.106 mm and operated at room temperature. The analysis involved several tests: a rotational rheology sweep test encompassing a range of 1 to 100 s^{-1} , a dynamic oscillatory test conducted within a shear stress range of 0.1 to 3000 Pa, and a frequency sweep test performed at frequencies spanning 0.01 to 100 Hz.

2.4. Direct ink writing

The printer used in this study is a pneumatic extrusion-based printer. In this printing system, there are three components, including a computer, a 3D printer (Axolotl Bio, Turkey), and an air compressor. The printhead is pneumatically actuated, so there are no mechanical parts inside. The first step is to turn on the air compressor so that the air in the air tank can be compressed to 72 psi. The dispenser's rotary spin is then activated so that an appropriate pressure can be prepared for printing the scaffold. To generate printing paths, click the 'Connect' button in the software interface to connect the computer and the 3D printer, and then choose the G-code file. The 3D printing process can be monitored in the software's interface window. On the printing system, a syringe and a changeable nozzle were mounted on the head to print along pre-designed patterns at an adjustable speed.

Strand widths are influenced by the size of the nozzles, the amount of dispensing pressure, and the speed of the printer head.

2.5. Thermogravimetric analysis (TGA)

Thermogravimetric analysis was employed to assess the thermal stability of the WPU printed meshes. The TGA/DTA instrument (Netsch STA 449 Jupiter, Germany) was utilized for this purpose. This technique monitors the degradation of the sample by measuring its weight using a microbalance during a heating scan. The samples were subjected to heating from 25 to 1000 °C in a nitrogen atmosphere (flow rate of 40 mL/min), with a scanning rate of 10 °C min⁻¹. By analyzing the weight loss and its derivative curves, two thermal parameters were determined.

2.6. Degradation and Swelling

The degradation rate of WPU was studied based on scaffolds weight loss in both phosphate buffer saline (PBS) solution and Dulbecco's Modified Eagle Medium (DMEM). A 15x15 mm² mesh was dissolved in two ml of PBS (pH= 7.4) and two ml of DMEM (pH= 8.3) for each period considered. The initial weight of the dry scaffold was recorded as W1 then put in PBS solution and DMEM media each and placed in a shaker incubator at 37 °C (90 rpm). At the intended intervals, scaffolds were taken out of the media to dry completely and weighed again, dried samples were recorded as W2. The degradation rate of the samples was calculated using Eq. (2.1).

$$\text{Degradation rate (\%)} = \frac{W_1 - W_2}{W_1} \times 100 \quad (2.1)$$

The swelling behavior of scaffolds was studied by submerging the WPU meshes in both PBS and DMEM media. Each mesh with size of 15x15 mm² was incubated in the above-mentioned media at 37 °C with a 90 rpm shake rate. Prior to immersing the scaffolds in the medium, their dry weight was determined, and samples were periodically taken out and weighed again after surface-adsorbed water was removed with filter paper. The Eq. (2.2) was used to calculate the swelling capacity.

$$\text{Swelling ratio (\%)} = \frac{W_{wet} - W_{dry}}{W_{dry}} \times 100 \quad (2.2)$$

Based on three replications, mean \pm standard deviation was expressed for each result.

2.7. Mechanical characterization

The mechanical properties of the scaffolds were analyzed using the Zwick Roell universal testing machine at a test speed of 10 mm/min, with a 10 KN load cell for the bending test and 200 N for the tensile test. The flexural properties of the scaffolds were determined by a three-point bending test according to the ASTM D-790 standard as shown schematically in Figure 4. Rectangular specimens were prepared for this experiment, $50.8 \times 12.7 \times T \text{ mm}^3$, where T is the thickness measured with a caliper. In all samples, ultimate tensile (UTS) and flexural strength (UFS) were determined as the stress reaching the highest value. The tensile and flexural modulus were calculated based on the slope of the straight-line portion of the stress–strain curves. Three replications were conducted, and each result was presented as a mean \pm standard deviation.

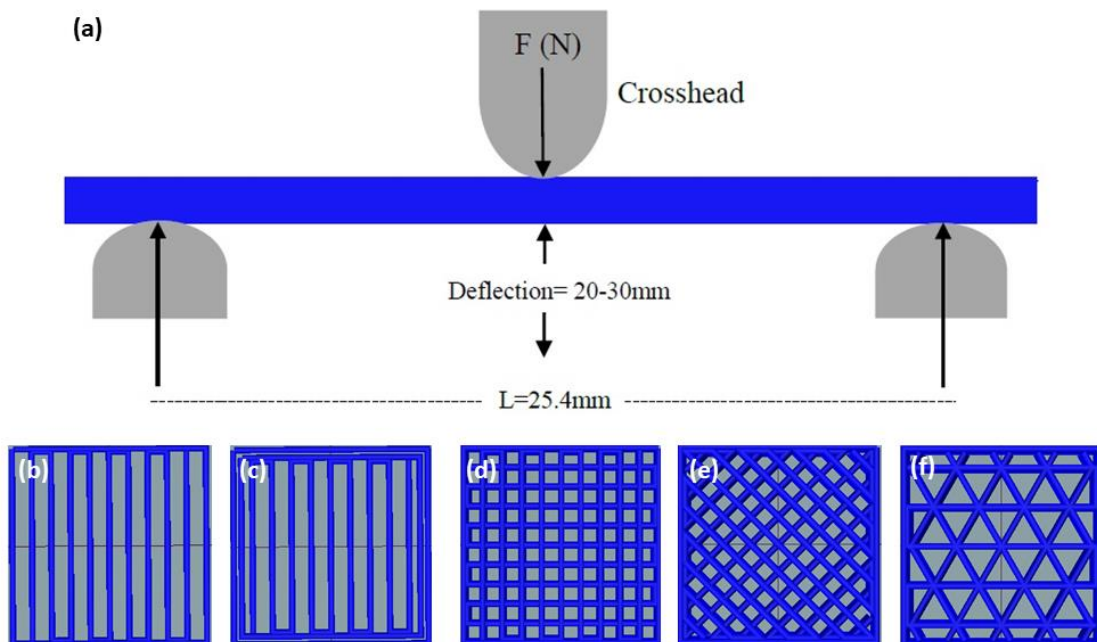


Figure 4. (a) Schematic illustration of three-point bending test of printed samples and the printed patterns used for mechanical tests, (b) aligned rectilinear, (c) aligned rectilinear with 2 walls, (d) rectilinear, (e) grid, (f) triangular

2.8. Drug release study

Ascorbic acid (AA) and tetracycline were chosen as the model drugs for studying the release profile from WPU scaffold. AA and tetracycline were individually added to the WPU ink. The mixture was gently stirred for 15 minutes and subsequently centrifuged at 3000 rpm for 10 minutes to achieve a homogeneous mixture. Release study of 0.5 wt.% of AA and 0.2 wt.% of tetracycline from printed WPU mesh evaluated at 37 °C within four days. Meshes with the size of 15x15 mm² submerged in 5 ml PBS (pH= 7.4) with constant shaking (210 rpm). 500 microliters of solution were withdrawn from each vial at predetermined time intervals and examined using UV–vis spectroscopy. To maintain the proper sink conditions, this was replaced with an equivalent amount of new buffer solution.

The UV spectrum at pH 7.4 showed a maximum absorption peak at 265 nm for AA and 271 nm for tetracycline. Using these wavelengths, the UV absorbance of different concentrations of AA at 265 nm and tetracycline at 271 nm was measured to create a standard curve. This standard curve was used to assess the drug release profile of the drug loaded WPU mesh.

Chapter 3

3. Results and discussions

3. Results and Discussions

The formulation of WPU inks involved the utilization of an aliphatic diisocyanate, (1,6 hexamethylene diisocyanate), as the hard segment in the WPU composition. Polyester polyols were selected as the soft segments based on their desirable properties such as high viscosity, chemical resistance, thermal stability, and oxidative stability. Three types of WPU inks, all having a high ionic content of 1.6% and solid content of 45%. The only variation among them was the ratio of the hard segment in the WPU main chain, with ratios of 16%, 18%, and 20%, labeled as WPU1, WPU2, and WPU3, respectively. These specific ink formulations were chosen for DIW printing due to their favorable viscosity, which eliminated the need for additional reinforcements during printing at ambient temperatures. By altering the ratio of the hard segment within the HDI-polyester polyol-based WPU inks, the aim was to investigate how these variations would impact the printability of the inks and the properties of the resulting scaffolds.

3.1. Rheological studies

The ratio of various components within the DIW inks formulation is pivotal in attaining the desired rheological behavior, ultimately facilitating optimal flow properties and printability. The results of the rheological measurements of the WPU inks are displayed in Figure 5. The viscosity of the synthesized WPU inks was studied by performing flow tests at increased shear rates. The viscosity curves followed a similar pattern for all WPU inks and exhibited shear thinning behavior. This behavior is desirable in DIW printing since it facilitates extrusion homogeneity along with rapid structural reconstruction [59]. The viscosities of WPU1, WPU2, and WPU3 inks at a shear rate of 1 s^{-1} were 279.08, 350.69, and 543 Pa·s. respectively. On the other hand, ink viscosity differences between shear rates 30 and 50 s^{-1} , associated with printing performance, were smaller than those at the shear rate 1 s^{-1} , varying between 7.7 and 17 Pa·s. It has been suggested that an ink viscosity range of 0.1 to 103 Pa·s is suitable for DIW printing [5], which is compatible with our WPU inks. The results showed that the viscosity increased with increasing particle size and hard segment from WPU1 to WPU3 as expected (Figure 5a).

In addition, oscillatory rheological analysis of the WPU inks (Figure 5b) showed that when shear stress is increased from 1 to 2000 Pa, the storage modulus of WPU with 18% (WPU2) and 20% (WPU3) hard segment dominated, revealing their solid-like behavior. As a result of the dominance of storage modulus, the printed pattern was guaranteed to retain its shape. The WPU ink with a 16% hard segment (WPU1) exhibited viscoelastic

properties different from these inks. WPU ink exhibited high storage modulus up until the shear stress of 612 Pa, after which the viscous characteristic dominates under higher shear stress conditions. In other words, WPU1 ink exhibited a yield stress point, which refers to the crossover point of the storage and loss modulus. However, the inks WPU2 and WPU3 did not display a yield stress point.

The ink's integrity was also evaluated through frequency sweep measurements involving analysis of both storage and loss modulus as shown in Figure 5c. Storage and loss modulus increased from WPU1 ink to WPU3 ink because of particle size and hard segment increase. A dominant elastic behavior was observed in WPU3, with G' always over G'' in all frequency ranges. WPU1 and WPU2 showed, however, crossings between G' and G'' at a higher frequency. This indicates a stronger dependency on frequency for viscoelastic behavior. At frequencies between 82.5 and 100 (Hz), WPU1 and WPU2 showed G'' greater than G' , indicating that viscous behavior was predominant.

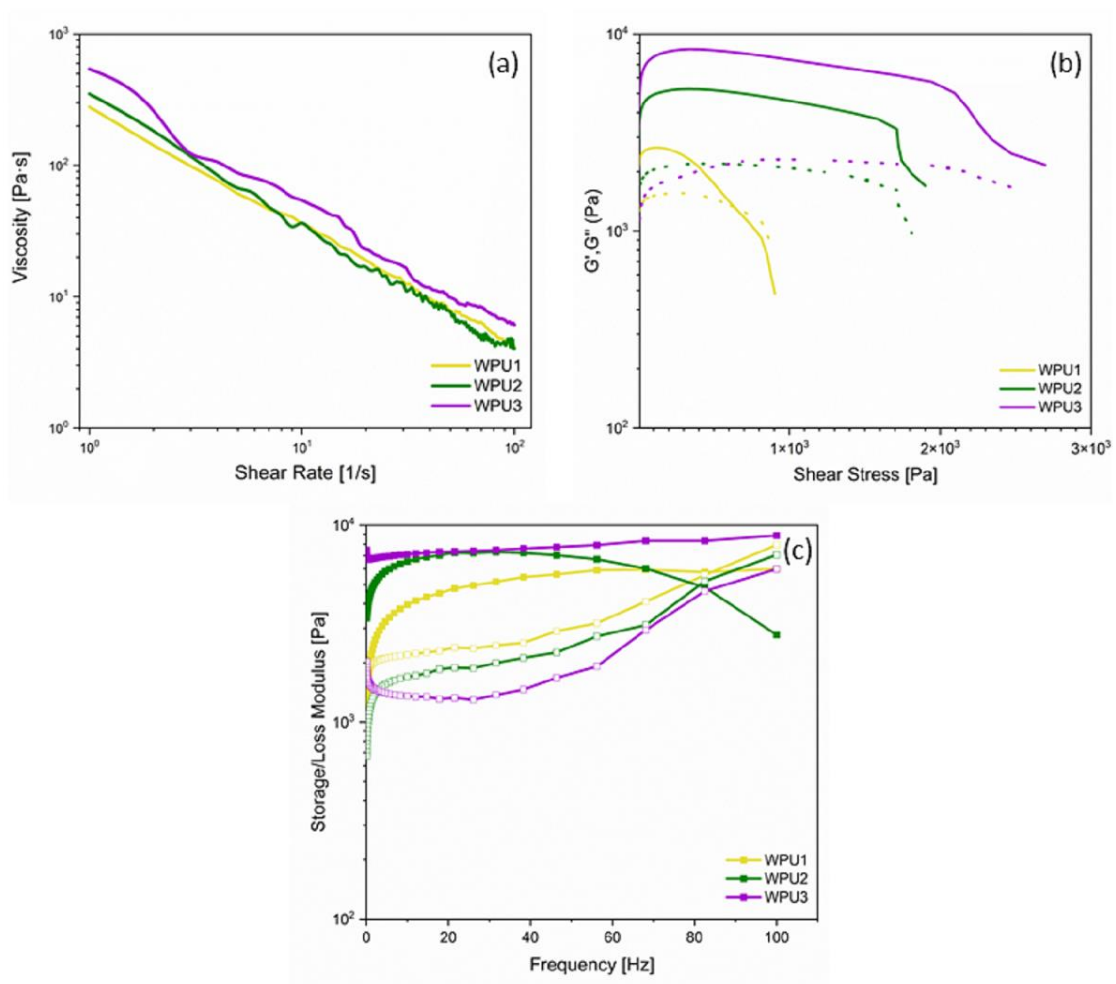


Figure 5. Rheological characteristics of the WPU inks with different hard segment contents, (a) dependence of viscosity to shear rate, (b) oscillatory rheological measurements of the inks including storage modulus (—) and loss modulus (...) as a function of shear stress, and (c) Storage (■) and loss (□) modulus as a function of frequency

Figure 6 shows the WPU scaffolds that were used to analyze the rheological characteristics of the inks in this work. It has been shown empirically that a storage modulus of over 103 Pa and large loss-elasticity modulus differences are critical to stabilizing a 3D structure with more than two layers [5]. This value was exceeded by the WPU inks we tested.

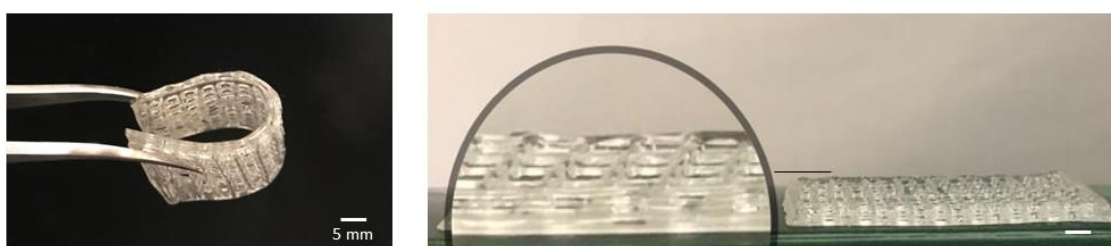


Figure 6. Images of a typical 3D-printed WPU scaffold analyzed in this study.

3.2. FTIR

The FTIR spectra of the WPU inks and the printed meshes were analyzed to identify WPU functional groups and the structural changes after the printing process and the results are shown in Figure 7. The bands observed in 1720–1740 cm^{-1} (C=O stretching) confirmed the presence of both polyol and urethane linkages. Bands at 1538–1560 cm^{-1} and 1230–1250 cm^{-1} (bending N-H and stretching C-N) further confirmed the presence of the urethane group. The band at 1140–1120 cm^{-1} indicated asymmetric C-O-C bonds in the urethane group. The band at 3300–3450 cm^{-1} was attributed to the N-H group of urethanes. Additionally, the absorbance in the range of 2790 to 2980 cm^{-1} was associated with the CH₂ vibrations of the polyester polyol group. In contrast, the absence of peaks within the 2280–2260 cm^{-1} ranges (associated with the –NCO group) confirmed the complete diisocyanate reaction during the synthesis process [59, 60].

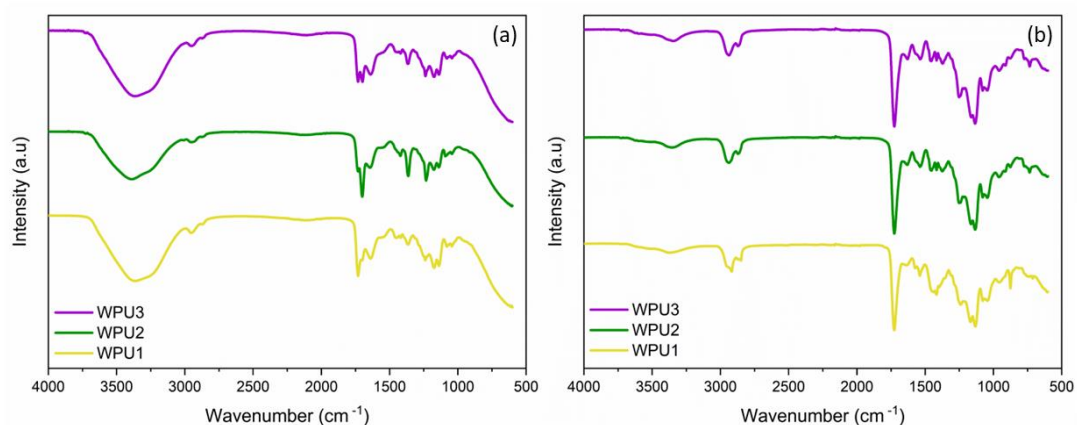


Figure 7. FTIR spectra of (a) WPU inks and (b) printed meshes.

In FTIR spectra of the drug loaded WPU ink, there are no peaks corresponding to ascorbic acid or tetracycline, indicating either no chemical bond formed between drugs and WPU or insufficient bonding due to low drug weight compared to WPU weight to suppress the bands [22, 61] (Figure 8). Without chemical bonding involved, erosion profile of the mesh, gradual breakdown or degradation, and mesh porosity govern the release kinetics of the drug from the mesh [62]. Although several methods exist for controlled drug release, the fabrication process often poses a drawback, making simple approaches necessary to generate drug release profiles [61]. Hence, WPU mesh offers a simple and efficient way to fabricate structures capable of controlled drug release.

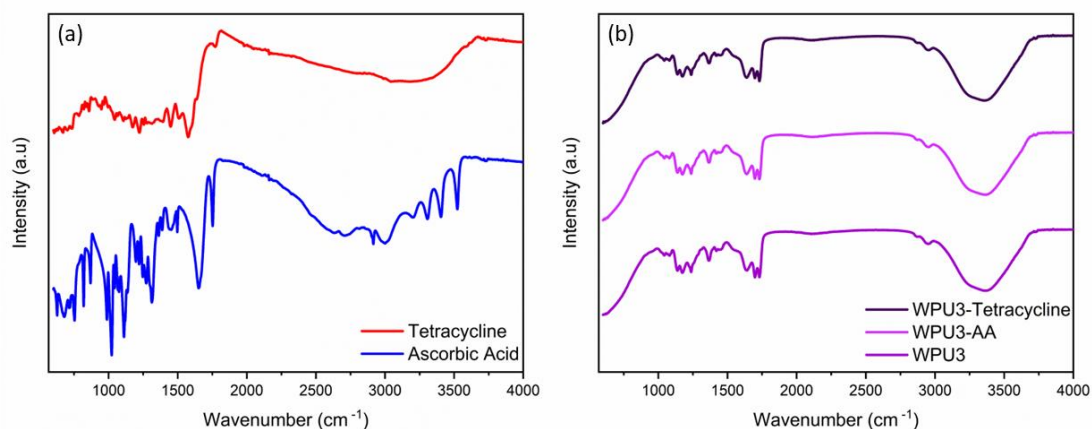


Figure 8. FTIR spectra of (a) drugs and (b) drug loaded WPU3.

3.3. Thermogravimetric analysis (TGA)

Figure 9 shows the thermogravimetric analysis (TG) and the derivative of the TG curve (DTG) for the thermal decomposition of WPU specimens with different hard segment contents. All the WPU samples exhibited identical thermal degradation characteristics. Regardless of the composition, three discernable peaks were observed in the DTG curves of the inks, indicative of three steps of thermal decomposition during the heating process. From the TG curves, it was revealed that the first step of weight loss occurred at the temperature range of 50 – 110 °C for the WPU1 and WPU2 with a maximum rate of degradation at about 75 °C, as indicated by the shallow peaks in the DTG curves and is attributed to the evaporation of the absorbed moisture by the inks during the processing. For the WPU3 ink, the onset temperature of the first weight loss step was shifted to a slightly higher temperature i.e., at 75 °C, with a maximum rate of mass loss at approximately 110 °C, possibly because of the increased number of hydrogen bonds between water molecules and the ink due to higher content of hard segment in WPU3. The thermograms revealed that the main step of thermal decomposition for the inks occurred at the temperature range of 300 – 500 °C as reflected by the sharp weight loss in TG traces of all the WPUs. The overall weight loss at this temperature range was shown to be the superimposition of two thermal degradation processes as evidenced by a sharp peak around 400 °C which was preceded by a peak shoulder at ca. 370 °C in the DTG curves. The decomposition process with a maximum rate of weight loss centered at 370 °C is related to the degradation of the hard segment through the dissociation of urethane linkages, upon which the urethane decomposes to the relevant alcohol and isocyanate units. This degradation step is accompanied by the liberation of carbon dioxide [63-66, 105-108]. The decomposition step with a maximum peak of around 400°C in DTG curves can be attributed to the thermal degradation of the polyester polyol as the soft segment of the inks [63, 64, 66].

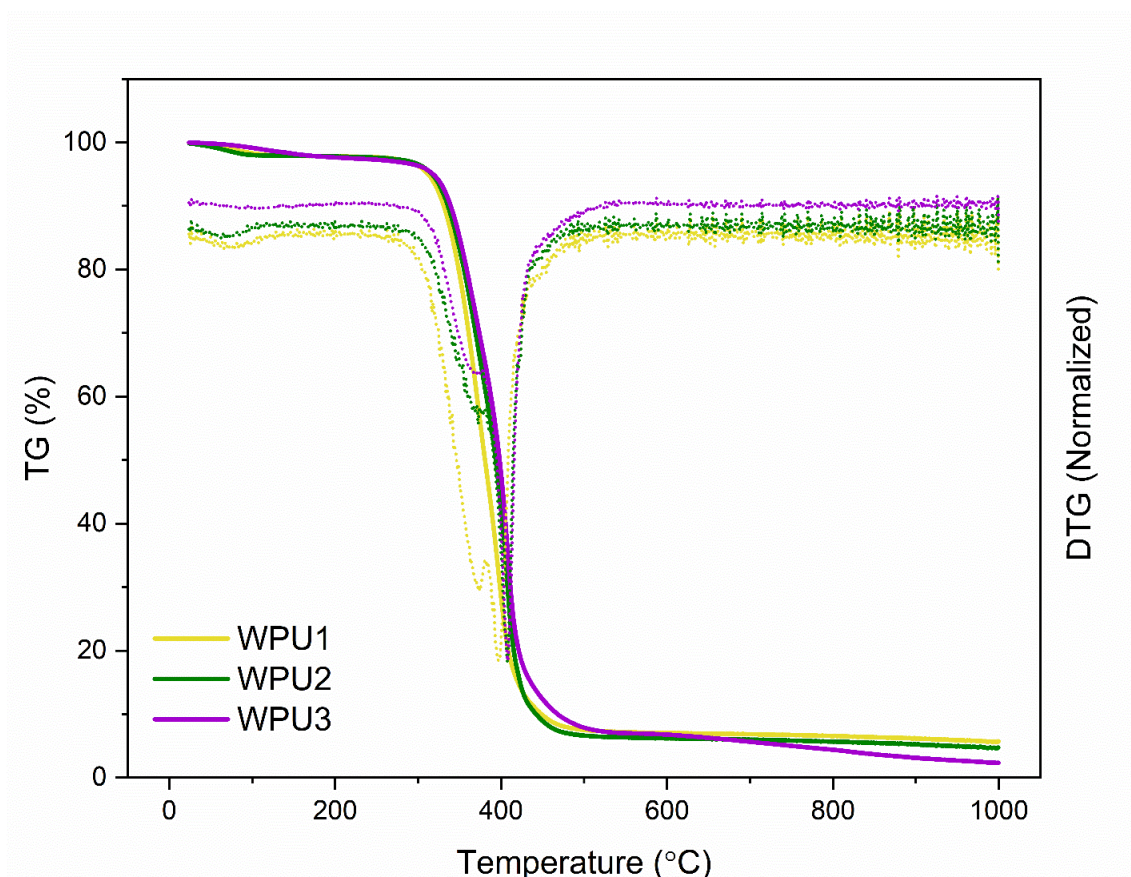


Figure 9. Thermogravimetry analysis for WPU mesh with different hard segment contents. Solid and dotted lines indicate TG and the corresponding derivatives of TG (DTG), respectively.

3.4. Degradation and Swelling

The degradation rate of the WPU scaffolds over time studied in PBS (pH=7.4) and DMEM (pH=8.3) media, Figure 10. The degradation analysis showed that while the weight loss increased gradually with degradation time in both media, more weight loss occurred in DMEM than in PBS, indicating that WPUs in DMEM degraded more rapidly. In DMEM, the degradation rate of WPU1 scaffolds reached 22.45 ± 0.2 % after 10 weeks, while in PBS it was 15.6 ± 0.2 %. WPU3 and WPU2 showed a slower degradation rate compared to WPU1, which could be explained by their higher hard segments in their structures compared to WPU1. The results of DMEM degradation testing showed that WPU1 scaffolds lost their structure, whereas WPU2 and 3 scaffolds retained structure and shape after 31 days.

WPU mesh degradation rate is influenced by its hard segment ratio, the higher the hard segment, the lower the degradation rate. Furthermore, for all the inks with different hard

segment contents, DMEM induced higher weight loss than PBS. Presence of the molecules in DMEM medium accelerates degradation and break ester bonds [67, 68], our results showed that, after 10 weeks of incubation, the pH value of the WPU degradation solution increased from 7.4 to 7.7 and from 8.3 to 8.8 in PBS and DMEM media, respectively.

WPU degradation is usually regulated and accelerated by adding highly degradable biomaterials, for example, lysine was added to WPU chains to make them degradable [60]. As PLGA replaces PCL in WPU scaffolds, degradation is accelerated, resulting in a weight loss of about 20% after four weeks [9]. Composites containing WPU and cellulose nanofibers degraded at 6.63% in PBS (28 days) and 33.6% in NaOH solution (5 days), whereas PU degraded at 2% in PBS after 28 days [30]. The degradation rate of PCL is very slow, reaching 1.3% after four weeks according to literature data [29].

In cases where the scaffold is used as a temporary support structure for tissue ingrowth, rapid degradation is necessary to accelerate cell infiltration and tissue formation. On the other hand, a slower degradation rate is preferred to provide long-term mechanical support where the scaffold should maintain its structural integrity and load-bearing capacity [69]. According to a study on rabbit knee osteochondral, articular cartilage regenerates completely after 84 days [70]. Approximately 30% weight loss after four weeks was suggested to be the appropriate degradation rate for cartilage regeneration [71]. It is recommended that scaffolds used in bone tissue engineering degrade within three to six months, depending on the anatomic site and applied load [29].

Moreover, the degradation test of WPU2-AA represented that the WPU scaffold containing ascorbic acid degraded faster than the pristine WPU scaffold (Figure 11). WPU2-AA scaffold degradation rate in PBS increased to $13.8 \pm 0.5\%$ for 5 mg/g AA, and to 48.56% for 10 mg/g AA. Ascorbic acid is hydrophilic, making WPU scaffolds more hydrophilic and accelerating degradation by increasing water-scaffold interaction [72]. Hence results showed that WPU scaffolds provide mechanical support, and their degradation rates can be controlled by adjusting the polymer hard segment ratio. A suitable biodegradation rate for different biomedical applications can be achieved by incorporating bioagents into WPU inks as well.

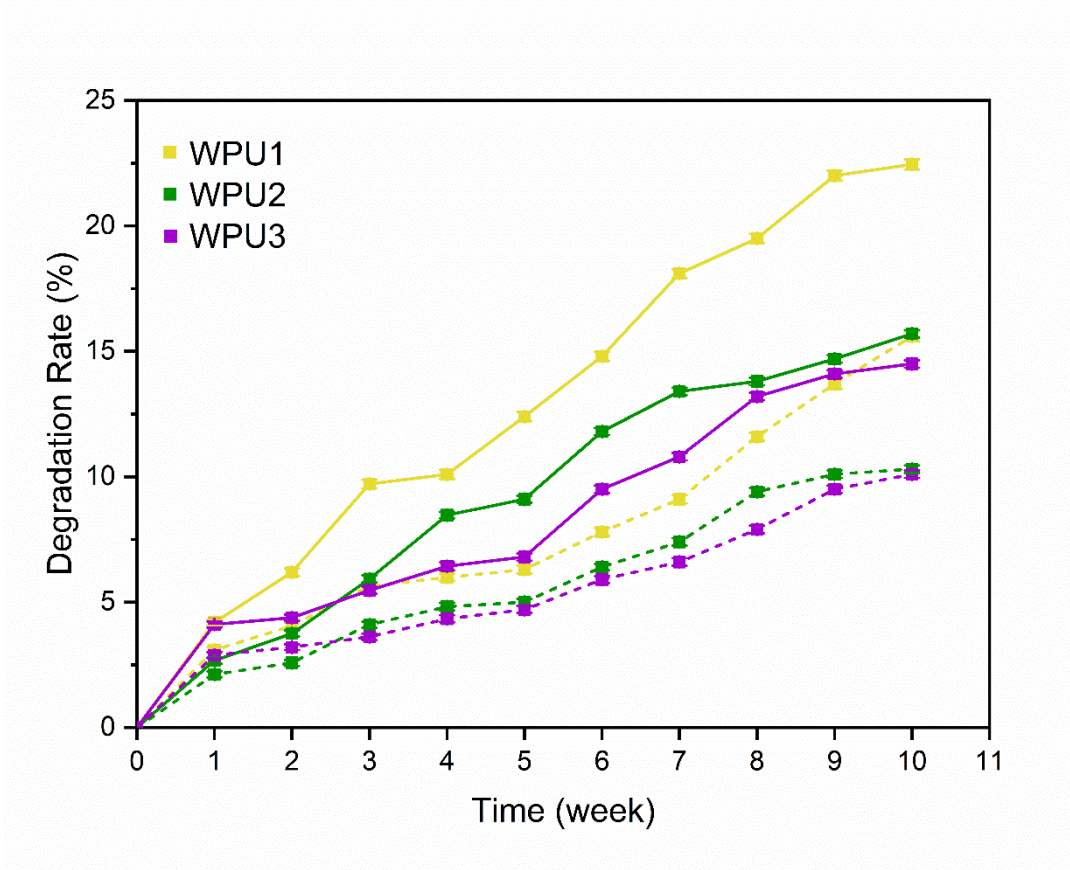


Figure 10. The degradation rate of WPU scaffolds in two media, PBS (dotted lines) and DMEM (solid lines)

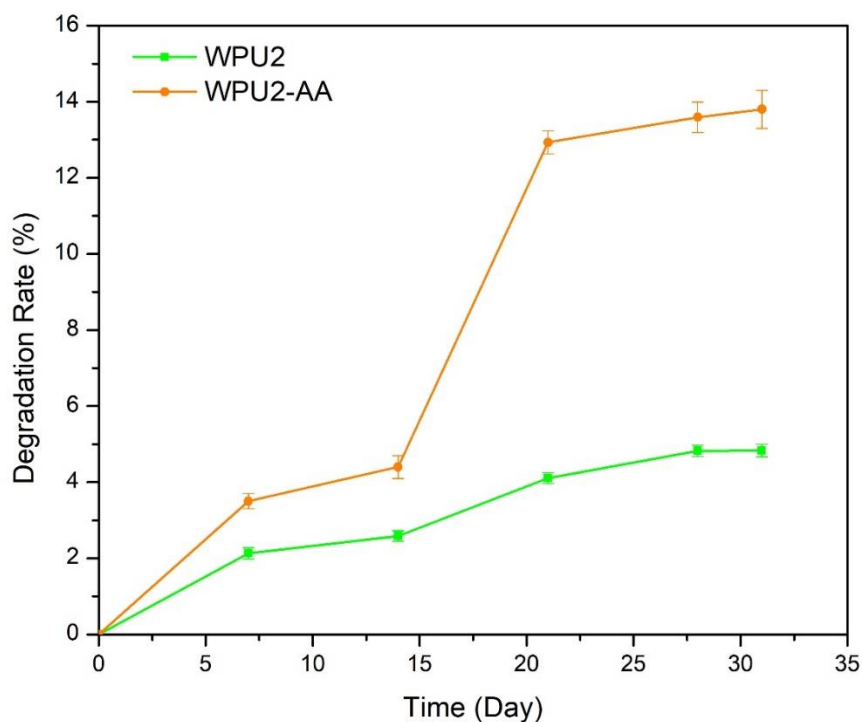


Figure 11. Degradation rate of WPU2 and WPU2-AA scaffolds in PBS

Because the swelling characteristics of biopolymers, that is the capability of absorbing liquid from the surrounding environment into the polymer chains without dissolving, play a vital role in cell adhesion, body fluid absorption, nutrient diffusion, and facilitated healing [41, 73], we also examined the swelling behavior of the WPU meshes. The swelling ratio of the WPUs as a function of time in both PBS and DMEM media is shown in Figure 12. The swelling ratio of the WPU scaffolds was found to increase by decreasing hard segments in the polymer chains. It was found that the inks in the DMEM medium undergo higher swelling than those in PBS [67, 68]. After immersion in DMEM medium for 10 weeks, swelling of $153 \pm 5\%$, $79 \pm 2\%$, and $59 \pm 2\%$ was observed for the WPU1, WPU2, and WPU3, respectively.

WPU contains ester, urea, and urethane linkages, which are susceptible to hydrolysis in the media. WPU mesh is hydrolytically degraded in aqueous solutions mainly through the hydrolysis of urethane and ester groups. Higher water absorption and swelling result in additional free volumes for mass transfer. Additionally, ester groups surround more

water molecules, which accelerates degradation [66, 74]. The results of scaffolds degradation and swelling analyses showed that WPU1 scaffolds lost their structure, whereas WPU2 and WPU3 scaffolds retained structure and shape after 30 days incubation in the media.

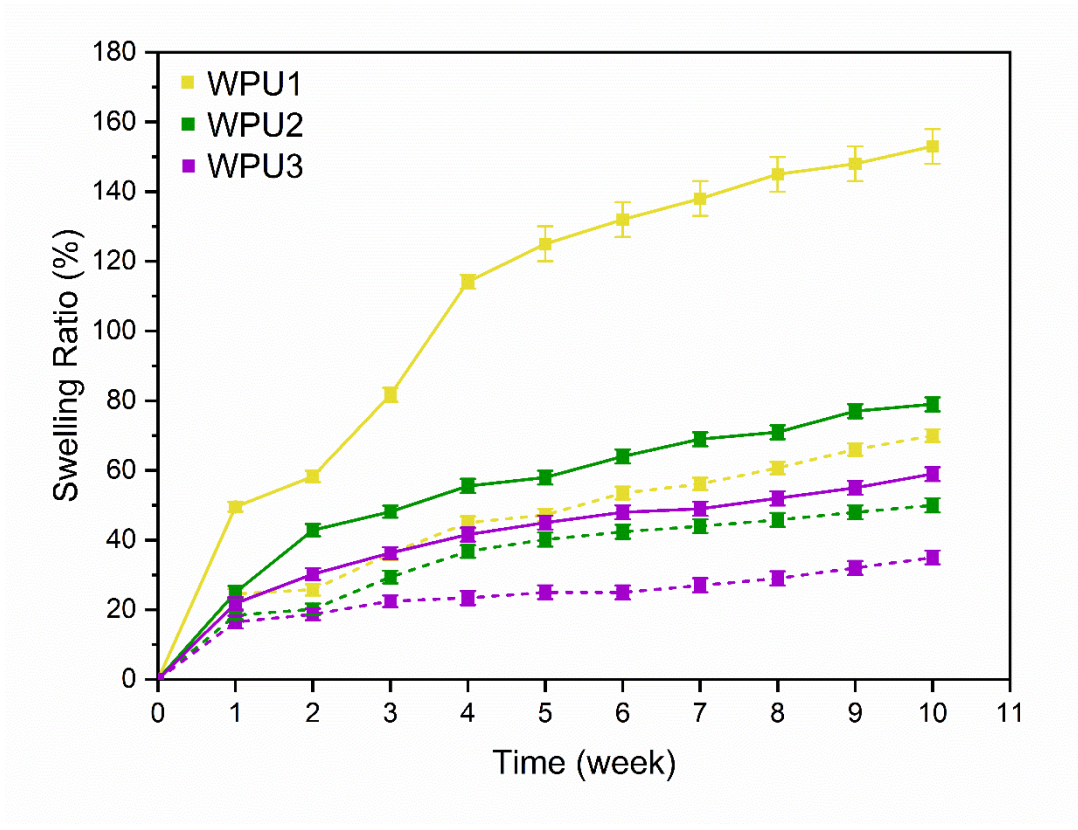


Figure 12. Swelling ratio of WPU scaffolds in two media, PBS (dotted lines) and DMEM (solid lines)

3.5. Mechanical studies

The influence of hard segment ratio of WPU inks on the strength and modulus of WPU scaffolds were studied. Additionally, the influence of infill densities and mesh design on the mechanical properties of the WPU scaffolds was investigated through both tensile and bending tests. The experimental setup included three distinct infill densities (20%, 35%, and 50%) and three patterns (rectilinear, grid, and triangular). Furthermore, the impact of

varying perimeters (1 and 2) was assessed in the tensile test, while the effect of different layers (2 and 4) was examined in the bending test.

Figure 14 shows the results of mechanical tests including both tensile stress-strain and flexural force-deformation graphs for WPU samples and Table 1 summarizes the mechanical properties of the printed samples. An increase in the hard segment ratio of WPU inks led to an increase in the modulus and ultimate strength of the printed samples during both tensile and bending loadings. The higher percentage of hard segments in the WPU backbone resulted in more rigid chains due to more urethane bonds and hydrogen bonding interactions. In other words, the augmented strength and modulus were primarily influenced by the greater proportion of aliphatic diisocyanate rigid units present in the WPU hard segment structure [28, 75, 76].

In addition, all infill percentages showed a consistent trend for each WPU type. However, specimens with higher infill percentages exhibited elevated modulus and strength values, indicating better strain resistance. This can be attributed to the denser material structure along printed lines achieved with higher infill percentages. As a result, the increased density enables the printed lines to effectively carry and distribute the load, leading to an overall enhancement in the strength of the samples [77].

During the tensile test, we also sought to understand the impact of perimeters, which refers to the number of walls surrounding the specimen circumference. These walls are used to maintain the shape of objects when loaded which also impacts the direction of deformation [77, 78]. Our results revealed that the samples with 2 perimeters exhibited higher strength than those with only 1 perimeter (Figure 13 a-c). Furthermore, for the WPU2 and WPU3 meshes, the sample with 35% infill and 2 perimeters demonstrated greater strength than the sample with 50% infill and 1 perimeter. In general, we observed that the influence of the number of walls on the strength of the specimen was relatively more significant than the infill densities, particularly at higher percentages of infill.

Regarding the mesh deformation under load, it was observed that the WPU1 ruptured after it reached ultimate tensile and flexural strength. Neither the WPU2 nor WPU3 printed materials ruptured under tensile and bending loads and retained their shape after being removed (Figure 13).

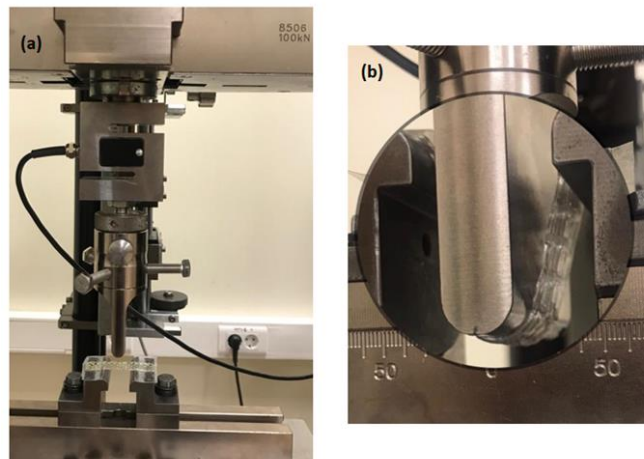
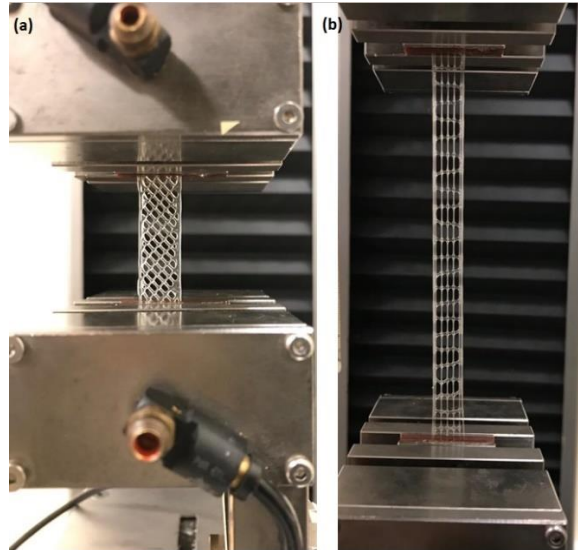
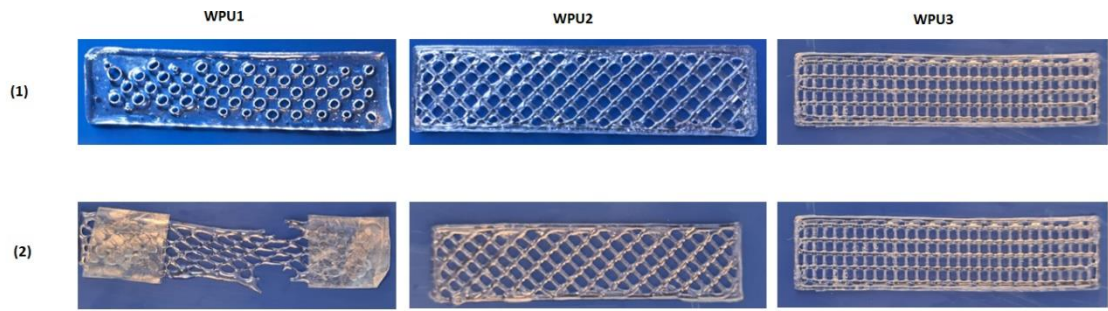


Figure 13. From top to bottom, deformation behavior of WPU scaffolds (1) before loading and (2) after loading.

WPU3 scaffolds under tensile test, (a) before loading and (b) during the loading.

WPU3 scaffold under 3-point bending test, (a) before loading and (b) during loading.

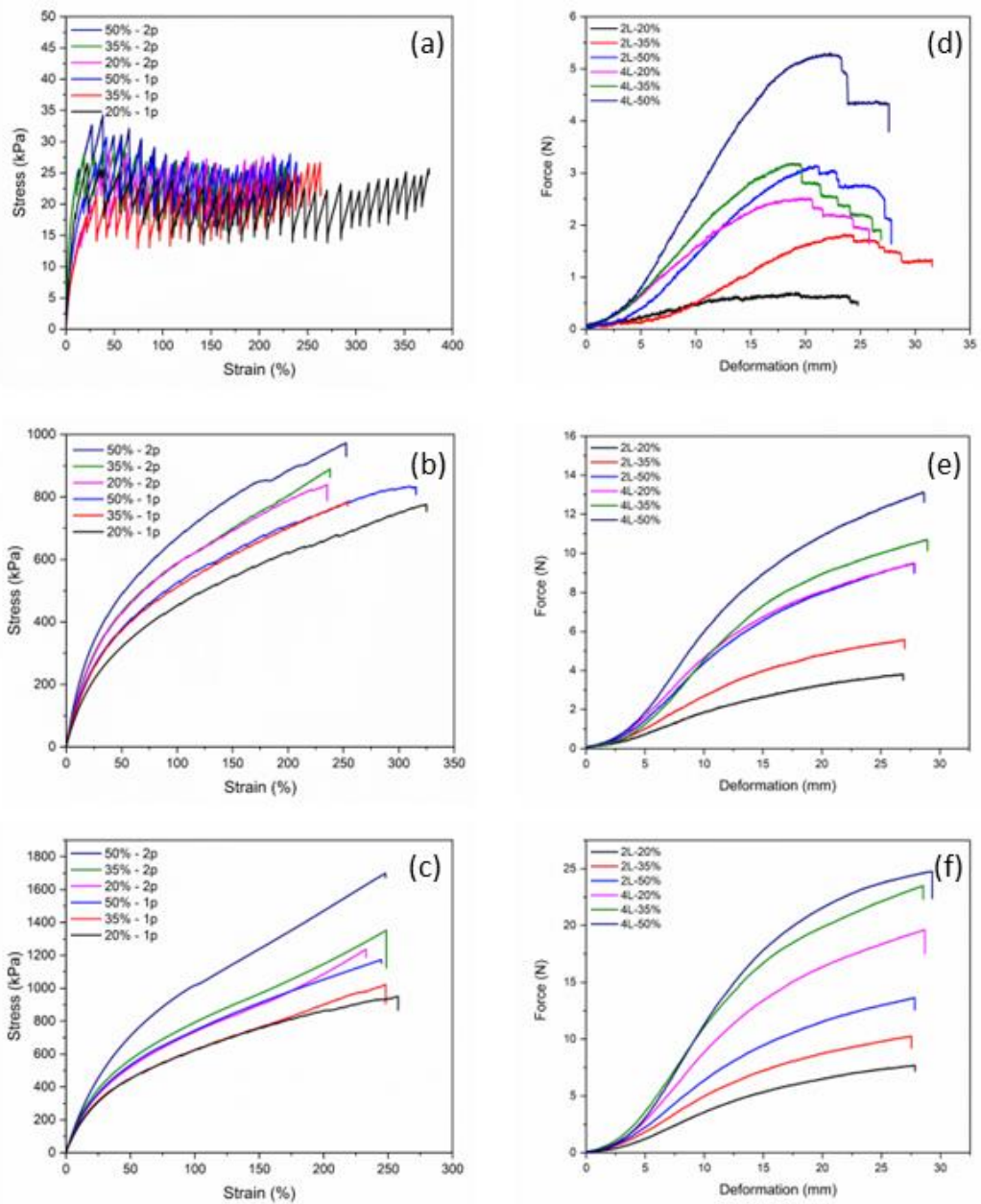


Figure 14. Stress-strain curves of the printed WPU scaffolds under tensile load (a-c), and the force-deformation diagrams under bending load (d-f).

Table 1. Mechanical properties of the printed meshes with different hard segment contents.

WPU Type	Mechanical Properties			
	Elastic Modulus (KPa)	Ultimate Tensile Strength (kPa)	Flexural Modulus (kPa)	Ultimate Flexural Strength (KPa)
WPU1	5.8 ± 1%	30 – 35	21.3 ± 1%	435 – 450
WPU2	19.7 ± 2%	830 – 860	56 ± 4%	910 – 940
WPU3	26 ± 2%	1220 – 1290	104 ± 4%	1650 – 1705

Figure 15 displays the effect of printed patterns on the mechanical properties of the tested samples under tensile and bending loads. In both the tensile and bending tests, the triangular pattern exhibited a superior modulus and strength compared to the other pattern. The performance of the infill pattern is influenced by the number of contact points it possesses. In this regard, the triangular infill pattern stands out due to its higher number of contact points per unit area. Furthermore, the triangular strands are printed on different axes, which enhances their resistance to the applied load [78, 79]. As a result, the triangular infill pattern exhibited better stiffness and structural integrity. The grid pattern, however, exhibited distinct behavior in both tests. In the bending test, the grid pattern demonstrated an improved flexural modulus compared to the rectilinear pattern while in the tensile test, the grid pattern displayed a decrease in the elastic modulus. This behavior can be explained by the relationship between the loading axis, the orientation of the strands, and the distribution of stress within the printed mesh subjected to the load. In fact, the behavior of the grid pattern strands under different loading conditions is attributed to their alignment relative to the axis of load. In the tensile load, the strands are more aligned along the axis of the load, making them prone to easier deformation. This results in a structure that is more susceptible to tensile forces. On the other hand, under bending load, the strands are oriented at approximately 45° relative to the bending load axis. This configuration increased the stiffness of the WPU mesh, as the strands are better able to resist bending forces. It is imperative to note that the performance of each pattern also depends on the materials used and the quality of the printed part. This is primarily due to the influence of factors such as layer adhesion, interlayer availability, and cohesion between internal patterns on the strength of printed samples [80, 81]. For instance, polyethylene terephthalate mesh with a triangle infill pattern exhibited lower tensile strength than those printed with a rectilinear pattern [80]. Conversely, for parts printed

with polylactic acid, the triangular pattern displayed better tensile strength compared to the rectilinear pattern [82].

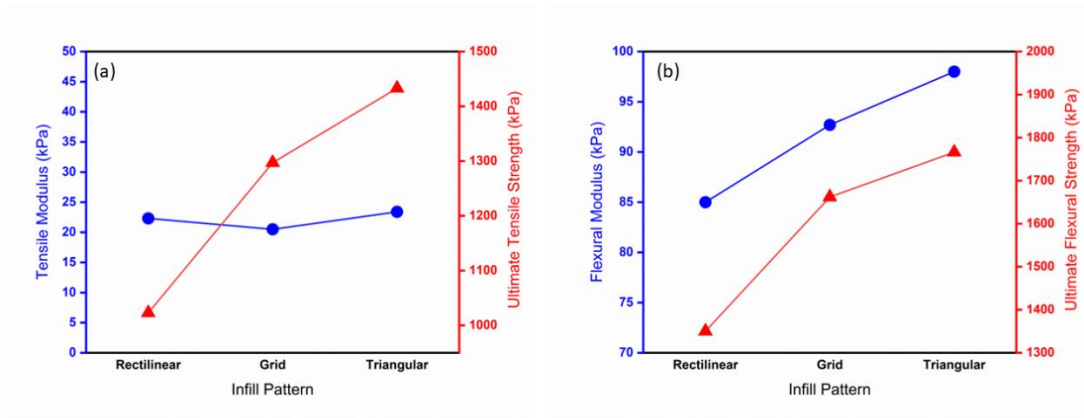


Figure 15. Effect of infill pattern on (a) tensile properties and (b) flexural properties of the ink with 20% hard segment (WPU3)

3.6. Drug release profile

The UV-vis absorbance spectra and release profile of ascorbic acid collected over four days are depicted in Figure 15. To investigate the influence of infill density on the drug release performance of the 3D printed mesh, two infill densities, 20% and 35%, were selected. A burst release of 26% was observed within the first 8 hours for the 20% infill density mesh, while the 35% infill density mesh exhibited a burst release of 35%, followed by a sustained release of the remaining 20% over a period of up to four days. AA release has almost ceased after 96 hours.

AA diffusion in water-based environments is unavoidable due to its low molecular weight and water solubility. It does not exhibit strong interactions with the polymer network in its surroundings. However, in a 3D-printed matrix, the presence of functional groups in the interactions between the vitamin and polymer allows for a dense structure. This compact structure enables the matrix to exhibit prolonged release behaviors of ascorbic acid [83]. The release of AA from a foam composite made of lactose-functionalized polyurea-urethanes was investigated. However, the study revealed that achieving a controlled release of AA from the foam was challenging. At a lower temperature of 25 °C, a very slow release of AA was observed and at a higher temperature of 37 °C, the complete release of ascorbic acid occurred within just 15 minutes [84]. Baniyadi et al. conducted a study on the release of ascorbic acid (AA) from DIW printed PVA-Cellulose

hydrogel using two different loading methods: direct loading and indirect loading. The results showed that direct loading resulted in a sustained release of AA, with approximately 80% of the loaded drug being released over a period of 8 hours. On the other hand, indirect loading led to a rapid release, with approximately 90% of the loaded drug being released within the first 60 minutes [85].

In the present study, the AA showed a controlled release path in a prolonged time than the release profiles of the above-mentioned studies. Therefore, the printed WPU matrix demonstrated high potential as a drug carrier for achieving a controlled release profile of AA over an extended period. Extended-release profiles enhance the therapeutic effectiveness of ascorbic acid at the intended site and reduce the risk of apoptosis associated with high doses. Additionally, utilizing a controlled release system in wound dressings provides a steady and efficient supply of ascorbic acid, facilitating improved wound healing [85, 86].

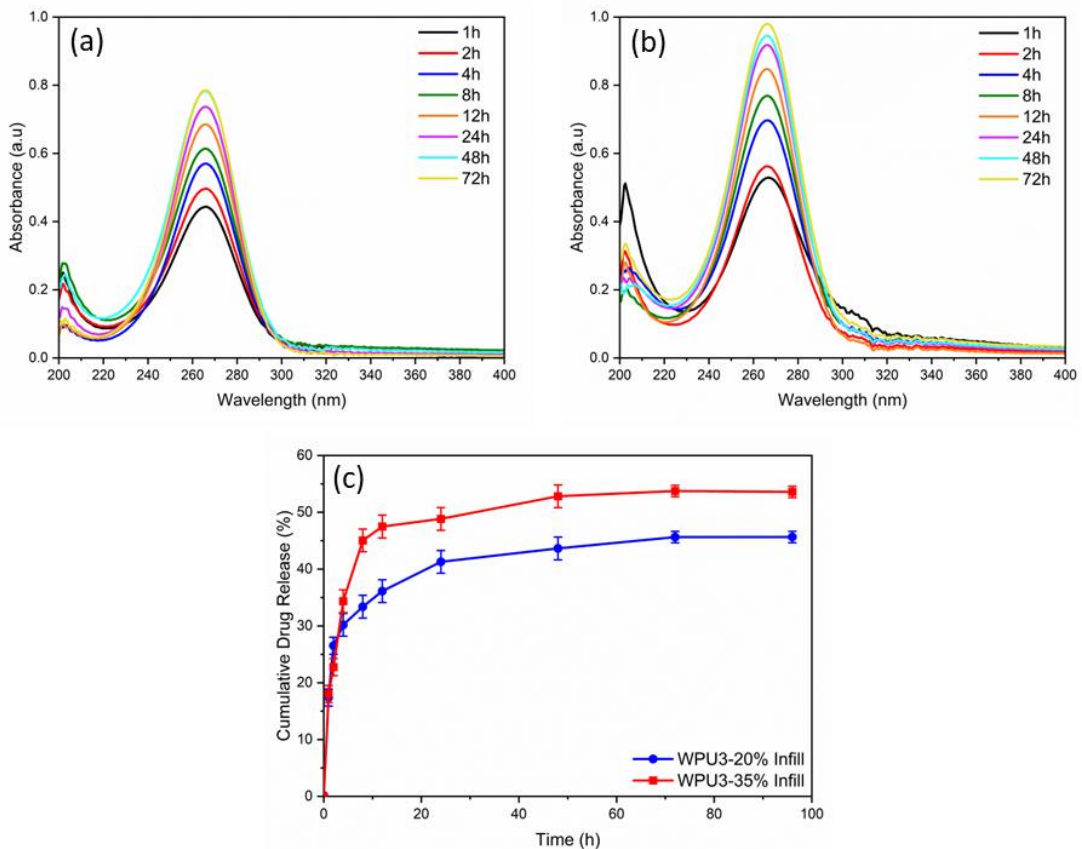


Figure 15. a) UV-vis spectra of AA loaded WPU 20 % infill, b) UV-vis spectra of AA loaded WPU 35 % infill, and c) AA release profiles from WPU mesh in PBS (pH=7.4) at room temperature

To further study the drug carrier potential of WPU scaffolds, tetracycline was chosen as the antibiotic of interest because of its broad-spectrum effectiveness against both gram-positive and gram-negative bacteria. However, it is crucial to acknowledge that administering high doses of different tetracycline forms intravenously has been associated with the development of acute fatty liver, which can lead to liver failure and potential mortality. Therefore, it is essential to establish a controlled release rate or mechanism for tetracycline to eliminate these risks.

Figure 16 illustrates the UV-vis absorbance spectra and release profile of tetracycline measured over a period of four days. After four days, the 20% infill mesh demonstrated a total release value of $72.39 \pm 2\%$, while the 35% infill mesh exhibited a total release value of $84.9 \pm 2\%$. Results of the in vitro release profiles describe an initial burst release of the drug (about 40-45%) followed by a slower release phase. In a study focusing on tetracycline hydrochloride-loaded PCL nanofibers, a comparable release pattern was observed, featuring a two-step release profile spanning 144 hours [87]. In another study, PLA implants were assessed for their ability to achieve a prolonged release path for tetracycline antibiotics for post-surgical infections. These implants were designed to sustain release over 1 month [88]. Tetracycline loaded PCL demonstrated that nearly all the drug was released within approximately 10 hours of incubation for PCL films. In contrast to the 2D PCL film, the release rate from 3D scaffolds exhibited a more sustained and slower profile, with only around 10% of the tetracycline released over a period of 70 hours [89].

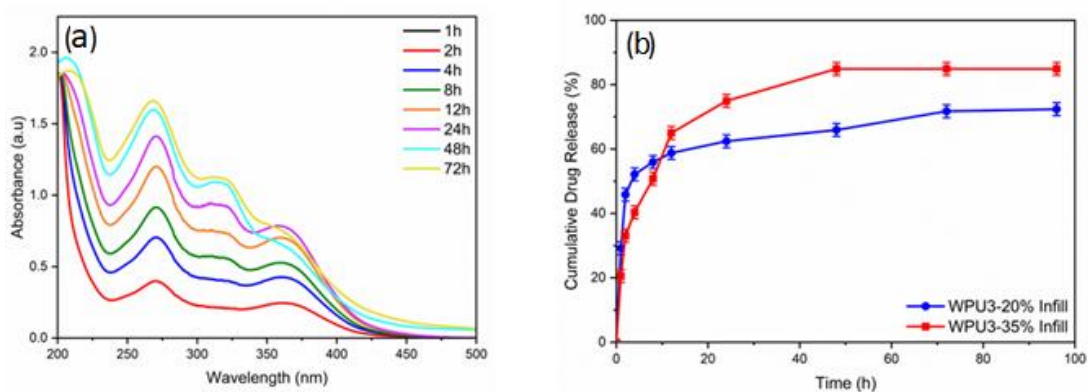


Figure 16. (a) UV-vis spectra of tetracycline loaded WPU3 and (b) Tetracycline release profiles from WPU mesh in PBS (pH=7.4) at 37°C temperature.

A variety of drugs have been released using WPU films, and several modifications including the addition of additives, the monomer ratio, and the dispersion of nanomaterials in polymer matrices have been employed to control the rate of drug release [44, 45, 90]. For example, methyl methacrylate was added to the WPU to prevent mitomycin c burst release from the WPU film. This resulted in the sustained release of 20.8 % of the anticancer drug after 30 hours and 57.3% after 10 days [44]. Here, through DIW 3D printing of WPU, we successfully achieved controlled drug release without additional steps for bioagent release regulation. It demonstrates the high potential of 3D-printed WPU scaffolds as effective and straightforward drug carriers.

Chapter 4

4 . Conclusion

4. Conclusion and future remarks

Direct ink writing technology offers significant advantages over traditional fabrication methods, such as ease of use, and environmental friendliness, particularly in biomedical applications. There is increasing demand for engineered anisotropic soft scaffolds in a wide range of fields, including soft tissue engineering, wound dressing, and biorobotics. This thesis aims to fabricate soft and robust matrices using DIW.

The study focused on selecting a series of waterborne polyurethane inks and investigating how print and process parameters affect the mechanical properties of printed scaffolds. Rheology studies demonstrated that the selected WPU inks possessed the necessary rheological properties for successful DIW without reinforcements.

Two mechanical characterizations, namely three-point bending and tensile tests, were conducted to evaluate the WPU scaffolds. The results indicated that print parameters, such as infill density, perimeters, and infill pattern, influenced the strength and modulus of the printed scaffolds, providing the potential for fabricating soft scaffolds with anisotropic and gradient properties.

The degradation and swelling properties of the printed parts exhibited rates comparable to previous WPU studies.

Additionally, DIW at room temperature demonstrated promising prospects for the pharmaceutical industry, particularly in the development of patient-tailored drugs with controlled drug release characteristics within mechanically stable matrices. The WPU printed matrix demonstrated the capability of controlled release profiles for two drug molecules, ascorbic acid, and tetracycline.

- Given the intriguing mechanical properties observed in the investigated WPU scaffolds and the significant influence of material composition on cellular responses, future research could focus on exploring the impact of WPU and bioactive loaded WPU scaffolds on a diverse array of cell types. This would provide valuable insights into cell behavior, such as proliferation, differentiation, and the overall potential for tissue regeneration facilitated by WPU-based scaffolds.

- Studying the release profile and kinetic behavior of other antibiotics and bioagents from WPU matrix, as well as exploring the synergistic effects of combining several types of drug molecules, holds significant promise for future research. These investigations can contribute to the development of improved drug delivery systems and facilitate the design of more effective therapeutic strategies.

References

- [1] P. Szymczyk-Ziółkowska, M. B. Łabowska, J. Detyna, I. Michalak, and P. Gruber, "A review of fabrication polymer scaffolds for biomedical applications using additive manufacturing techniques," *Biocybernetics and Biomedical Engineering*, vol. 40, no. 2, pp. 624-638, 2020, doi: 10.1016/j.bbe.2020.01.015.
- [2] S. Bose, D. Ke, H. Sahasrabudhe, and A. Bandyopadhyay, "Additive manufacturing of biomaterials," *Prog Mater Sci*, vol. 93, pp. 45-111, Apr 2018, doi:10.1016/j.pmatsci.2017.08.003.
- [3] E. A. Guzzi and M. W. Tibbitt, "Additive Manufacturing of Precision Biomaterials," *Adv Mater*, vol. 32, no. 13, p. e1901994, Apr 2020, doi: 10.1002/adma.201901994.
- [4] T. D. Ngo, A. Kashani, G. Imbalzano, K. T. Q. Nguyen, and D. Hui, "Additive manufacturing (3D printing): A review of materials, methods, applications and challenges," *Composites Part B: Engineering*, vol. 143, pp. 172-196, 2018, doi: 10.1016/j.compositesb.2018.02.012.
- [5] L. Li, Q. Lin, M. Tang, A. J. E. Duncan, and C. Ke, "Advanced Polymer Designs for Direct-Ink-Write 3D Printing," *Chemistry*, vol. 25, no. 46, pp. 10768-10781, Aug 14 2019, doi: 10.1002/chem.201900975.
- [6] M. Saadi *et al.*, "Direct Ink Writing: A 3D Printing Technology for Diverse Materials," *Adv Mater*, vol. 34, no. 28, p. e2108855, Jul 2022, doi: 10.1002/adma.202108855.
- [7] W. Bao *et al.*, "Advancements and Frontiers in the High Performance of Natural Hydrogels for Cartilage Tissue Engineering," *Front Chem*, vol. 8, p. 53, 2020, doi: 10.3389/fchem.2020.00053.
- [8] N. Di Marzio, D. Eglin, T. Serra, and L. Moroni, "Bio-Fabrication: Convergence of 3D Bioprinting and Nano-Biomaterials in Tissue Engineering and Regenerative Medicine," *Front Bioeng Biotechnol*, vol. 8, p. 326, 2020, doi: 10.3389/fbioe.2020.00326.
- [9] B. Du *et al.*, "A waterborne polyurethane 3D scaffold containing PLGA with a controllable degradation rate and an anti-inflammatory effect for potential applications in neural tissue repair," *J Mater Chem B*, vol. 8, no. 20, pp. 4434-4446, May 27 2020, doi: 10.1039/d0tb00656d.
- [10] F. P. W. Melchels, M. A. N. Domingos, T. J. Klein, J. Malda, P. J. Bartolo, and D. W. Hutmacher, "Additive manufacturing of tissues and organs," *Progress in Polymer Science*, vol. 37, no. 8, pp. 1079-1104, 2012, doi: 10.1016/j.progpolymsci.2011.11.007.
- [11] M. P. Lutolf, P. M. Gilbert, and H. M. Blau, "Designing materials to direct stem-cell fate," *Nature*, vol. 462, no. 7272, pp. 433-41, Nov 26 2009, doi: 10.1038/nature08602.

- [12] J. Vadillo, I. Larraza, T. Calvo-Correas, N. Gabilondo, C. Derail, and A. Eceiza, "Design of a Waterborne Polyurethane-Urea Ink for Direct Ink Writing 3D Printing," *Materials (Basel)*, vol. 14, no. 12, Jun 14 2021, doi: 10.3390/ma14123287.
- [13] L. Xiaorui *et al.*, "1Biomaterial inks for extrusion-based 3D bioprinting: Property, classification, modification, and selection," *Int J Bioprint*, vol. 9, no. 2, p. 649, 2023, doi: 10.18063/ijb.v9i2.649.
- [14] H. Li, Y. J. Tan, S. Liu, and L. Li, "Three-Dimensional Bioprinting of Oppositely Charged Hydrogels with Super Strong Interface Bonding," *ACS Appl Mater Interfaces*, vol. 10, no. 13, pp. 11164-11174, Apr 4 2018, doi: 10.1021/acsami.7b19730.
- [15] A. Johnston and A. Callanan, "Recent Methods for Modifying Mechanical Properties of Tissue-Engineered Scaffolds for Clinical Applications," *Biomimetics (Basel)*, vol. 8, no. 2, May 16 2023, doi: 10.3390/biomimetics8020205.
- [16] C. Xu, Y. Huang, L. Tang, and Y. Hong, "Low-Initial-Modulus Biodegradable Polyurethane Elastomers for Soft Tissue Regeneration," *ACS Appl Mater Interfaces*, vol. 9, no. 3, pp. 2169-2180, Jan 25 2017, doi: 10.1021/acsami.6b15009.
- [17] G. Zhang *et al.*, "In Vitro Effects of Waterborne Polyurethane 3D Scaffolds Containing Poly(lactic-co-glycolic acid)s of Different Lactic Acid/Glycolic Acid Ratios on the Inflammatory Response," *Polymers (Basel)*, vol. 15, no. 7, Apr 4 2023, doi: 10.3390/polym15071786.
- [18] E. Tomecka, M. Wojasinski, E. Jastrzebska, M. Chudy, T. Ciach, and Z. Brzozka, "Poly(l-lactic acid) and polyurethane nanofibers fabricated by solution blow spinning as potential substrates for cardiac cell culture," *Mater Sci Eng C Mater Biol Appl*, vol. 75, pp. 305-316, Jun 1 2017, doi: 10.1016/j.msec.2017.02.055.
- [19] K. A and L. A, "Mechanical Behaviour of Skin: A Review," *Journal of Material Science & Engineering*, vol. 5, no. 4, 2016, doi: 10.4172/2169-0022.1000254.
- [20] Y. T. Wen, N. T. Dai, and S. H. Hsu, "Biodegradable water-based polyurethane scaffolds with a sequential release function for cell-free cartilage tissue engineering," *Acta Biomater*, vol. 88, pp. 301-313, Apr 1 2019, doi: 10.1016/j.actbio.2019.02.044.
- [21] O. Janouskova, "Synthetic polymer scaffolds for soft tissue engineering," *Physiol Res*, vol. 67, no. Suppl 2, pp. S335-S348, Oct 30 2018, doi: 10.33549/physiolres.933983.
- [22] J. Dominguez-Robles *et al.*, "3D Printing of Drug-Loaded Thermoplastic Polyurethane Meshes: A Potential Material for Soft Tissue Reinforcement in Vaginal Surgery," *Pharmaceutics*, vol. 12, no. 1, Jan 13 2020, doi: 10.3390/pharmaceutics12010063.
- [23] Z. Feng *et al.*, "A novel waterborne polyurethane with biodegradability and high flexibility for 3D printing," *Biofabrication*, vol. 12, no. 3, p. 035015, May 12 2020, doi: 10.1088/1758-5090/ab7de0.

- [24] R. Pugliese, B. Beltrami, S. Regondi, and C. Lunetta, "Polymeric biomaterials for 3D printing in medicine: An overview," *Annals of 3D Printed Medicine*, vol. 2, 2021, doi: 10.1016/j.stlm.2021.100011.
- [25] K. C. Hung, C. S. Tseng, L. G. Dai, and S. H. Hsu, "Water-based polyurethane 3D printed scaffolds with controlled release function for customized cartilage tissue engineering," *Biomaterials*, vol. 83, pp. 156-68, Mar 2016, doi: 10.1016/j.biomaterials.2016.01.019.
- [26] R. Sinha *et al.*, "A hybrid additive manufacturing platform to create bulk and surface composition gradients on scaffolds for tissue regeneration," *Nat Commun*, vol. 12, no. 1, p. 500, Jan 21 2021, doi: 10.1038/s41467-020-20865-y.
- [27] I. Larraza *et al.*, "The effect of the carboxylation degree on cellulose nanofibers and waterborne polyurethane/cellulose nanofiber nanocomposites properties," *Polymer Degradation and Stability*, vol. 173, 2020, doi: 10.1016/j.polymdegradstab.2020.109084.
- [28] D. Anıl, E. Berksun, A. Durmuş-Sayar, E. B. Sevinis, Özbulut, and S. Ünal, "Recent advances in waterborne polyurethanes and their nanoparticle-containing dispersions," in *Handbook of Waterborne Coatings*, 2020, pp. 249-302.
- [29] M. Boffito *et al.*, "Custom-Made Poly(urethane) Coatings Improve the Mechanical Properties of Bioactive Glass Scaffolds Designed for Bone Tissue Engineering," *Polymers (Basel)*, vol. 14, no. 1, Dec 31 2021, doi: 10.3390/polym14010151.
- [30] R. D. Chen, C. F. Huang, and S. H. Hsu, "Composites of waterborne polyurethane and cellulose nanofibers for 3D printing and bioapplications," *Carbohydr Polym*, vol. 212, pp. 75-88, May 15 2019, doi: 10.1016/j.carbpol.2019.02.025.
- [31] C. Wang, Y. Zheng, K. Qiao, Y. Xie, and X. Zhou, "An environmentally friendly preparation and characterization of waterborne polyurethane hydrogels by polyvinyl alcohol physical cross-linking to improve water absorption," *RSC Advances*, vol. 5, no. 90, pp. 73882-73891, 2015, doi: 10.1039/c5ra11109a.
- [32] C.-T. Hsieh, C.-Y. Liao, N.-T. Dai, C.-S. Tseng, B. L. Yen, and S.-h. Hsu, "3D printing of tubular scaffolds with elasticity and complex structure from multiple waterborne polyurethanes for tracheal tissue engineering," *Applied Materials Today*, vol. 12, pp. 330-341, 2018, doi: 10.1016/j.apmt.2018.06.004.
- [33] W. Lin *et al.*, "Aligned 3D porous polyurethane scaffolds for biological anisotropic tissue regeneration," *Regen Biomater*, vol. 7, no. 1, pp. 19-27, Feb 2020, doi: 10.1093/rb/rbz031.
- [34] A. Schwab, R. Levato, M. D'Este, S. Piluso, D. Eglin, and J. Malda, "Printability and Shape Fidelity of Bioinks in 3D Bioprinting," *Chem Rev*, vol. 120, no. 19, pp. 11028-11055, Oct 14 2020, doi: 10.1021/acs.chemrev.0c00084.

- [35] Z. Jiang, B. Diggle, M. L. Tan, J. Viktorova, C. W. Bennett, and L. A. Connal, "Extrusion 3D Printing of Polymeric Materials with Advanced Properties," *Adv Sci (Weinh)*, vol. 7, no. 17, p. 2001379, Sep 2020, doi: 10.1002/advs.202001379.
- [36] S. Jang *et al.*, "Effect of material extrusion process parameters on filament geometry and inter-filament voids in as-fabricated high solids loaded polymer composites," *Additive Manufacturing*, vol. 47, 2021, doi: 10.1016/j.addma.2021.102313.
- [37] B. Zhang, R. Cristescu, D. B. Chrisey, and R. J. Narayan, "Solvent-based Extrusion 3D Printing for the Fabrication of Tissue Engineering Scaffolds," *Int J Bioprint*, vol. 6, no. 1, p. 211, 2020, doi: 10.18063/ijb.v6i1.211.
- [38] J. P. Caffrey *et al.*, "Flexural properties of native and tissue-engineered human septal cartilage," *Otolaryngol Head Neck Surg*, vol. 148, no. 4, pp. 576-81, Apr 2013, doi: 10.1177/0194599812474228.
- [39] B. Laycock *et al.*, "Lifetime prediction of biodegradable polymers," *Progress in Polymer Science*, vol. 71, pp. 144-189, 2017, doi: 10.1016/j.progpolymsci.2017.02.004.
- [40] M. U. A. Khan, S. I. A. Razak, M. N. M. Ansari, R. M. Zulkifli, N. Ahmad Zawawi, and M. Arshad, "Development of Biodegradable Bio-Based Composite for Bone Tissue Engineering: Synthesis, Characterization and In Vitro Biocompatible Evaluation," *Polymers (Basel)*, vol. 13, no. 21, Oct 20 2021, doi: 10.3390/polym13213611.
- [41] K. Bankoti *et al.*, "Accelerated healing of full thickness dermal wounds by macroporous waterborne polyurethane-chitosan hydrogel scaffolds," *Mater Sci Eng C Mater Biol Appl*, vol. 81, pp. 133-143, Dec 1 2017, doi: 10.1016/j.msec.2017.07.018.
- [42] I. R. Calori, G. Braga, P. d. C. C. de Jesus, H. Bi, and A. C. Tedesco, "Polymer scaffolds as drug delivery systems," *European Polymer Journal*, vol. 129, 2020, doi: 10.1016/j.eurpolymj.2020.109621.
- [43] E. Mathew, G. Pitzanti, E. Larraneta, and D. A. Lamprou, "3D Printing of Pharmaceuticals and Drug Delivery Devices," *Pharmaceutics*, vol. 12, no. 3, Mar 15 2020, doi: 10.3390/pharmaceutics12030266.
- [44] A. Bahadur, A. Saeed, M. Shoaib, S. Iqbal, and S. Anwer, "Modulating the burst drug release effect of waterborne polyurethane matrix by modifying with polymethylmethacrylate," *Journal of Applied Polymer Science*, vol. 136, no. 13, 2019, doi: 10.1002/app.47253.
- [45] I. R. S. Vieira *et al.*, "Transdermal progesterone delivery study from waterborne poly(urethane-urea)s nanocomposites films based on montmorillonite clay and reduced graphene oxide," *Journal of Drug Delivery Science and Technology*, vol. 60, 2020, doi: 10.1016/j.jddst.2020.101873.

- [46] A. Bahadur *et al.*, "Biocompatible waterborne polyurethane-urea elastomer as intelligent anticancer drug release matrix: A sustained drug release study," *Reactive and Functional Polymers*, vol. 119, pp. 57-63, 2017, doi: 10.1016/j.reactfunctpolym.2017.08.001.
- [47] M. Shoaib *et al.*, "Relationship of hard segment concentration in polyurethane-urea elastomers with mechanical, thermal and drug release properties," *Journal of Drug Delivery Science and Technology*, vol. 37, pp. 88-96, 2017, doi: 10.1016/j.jddst.2016.12.003.
- [48] E. Mathew *et al.*, "Fused Deposition Modeling as an Effective Tool for Anti-Infective Dialysis Catheter Fabrication," *ACS Biomater Sci Eng*, vol. 5, no. 11, pp. 6300-6310, Nov 11 2019, doi: 10.1021/acsbio.2019.01185.
- [49] K. J. Rambhia and P. X. Ma, "Controlled drug release for tissue engineering," *J Control Release*, vol. 219, pp. 119-128, Dec 10 2015, doi: 10.1016/j.jconrel.2015.08.049.
- [50] D. K. Tan, M. Maniruzzaman, and A. Nokhodchi, "Advanced Pharmaceutical Applications of Hot-Melt Extrusion Coupled with Fused Deposition Modelling (FDM) 3D Printing for Personalised Drug Delivery," *Pharmaceutics*, vol. 10, no. 4, Oct 24 2018, doi: 10.3390/pharmaceutics10040203.
- [51] B. Zhang, A. K. Nguyen, R. J. Narayan, and J. Huang, "Direct ink writing of vancomycin-loaded polycaprolactone/ polyethylene oxide/ hydroxyapatite 3D scaffolds," *Journal of the American Ceramic Society*, vol. 105, no. 3, pp. 1821-1840, 2021, doi: 10.1111/jace.18048.
- [52] R. Ajdary *et al.*, "Direct Ink Writing of Biocompatible Nanocellulose and Chitosan Hydrogels for Implant Mesh Matrices," *ACS Polym Au*, vol. 2, no. 2, pp. 97-107, Apr 13 2022, doi: 10.1021/acspolymersau.1c00045.
- [53] V. Vivcharenko and A. Przekora, "Modifications of Wound Dressings with Bioactive Agents to Achieve Improved Pro-Healing Properties," *Applied Sciences*, vol. 11, no. 9, 2021, doi: 10.3390/app11094114.
- [54] M. Attia, E. A. Essa, R. M. Zaki, and A. A. Elkordy, "An Overview of the Antioxidant Effects of Ascorbic Acid and Alpha Lipoic Acid (in Liposomal Forms) as Adjuvant in Cancer Treatment," *Antioxidants (Basel)*, vol. 9, no. 5, Apr 25 2020, doi: 10.3390/antiox9050359.
- [55] R. Dagher and P. Drogui, "Tetracycline antibiotics in the environment: a review," *Environmental Chemistry Letters*, vol. 11, no. 3, pp. 209-227, 2013, doi: 10.1007/s10311-013-0404-8.
- [56] M. Lin *et al.*, "Synergistic Effect of Co-Delivering Ciprofloxacin and Tetracycline Hydrochloride for Promoted Wound Healing by Utilizing Coaxial PCL/Gelatin Nanofiber Membrane," *Int J Mol Sci*, vol. 23, no. 3, Feb 8 2022, doi: 10.3390/ijms23031895.

- [57] F. Nainu *et al.*, "Pharmaceutical Approaches on Antimicrobial Resistance: Prospects and Challenges," *Antibiotics (Basel)*, vol. 10, no. 8, Aug 14 2021, doi: 10.3390/antibiotics10080981.
- [58] M. Ranjbar-Mohammadi, M. Zamani, M. P. Prabhakaran, S. H. Bahrami, and S. Ramakrishna, "Electrospinning of PLGA/gum tragacanth nanofibers containing tetracycline hydrochloride for periodontal regeneration," *Mater Sci Eng C Mater Biol Appl*, vol. 58, pp. 521-31, Jan 1 2016, doi: 10.1016/j.msec.2015.08.066.
- [59] J. Vellido, I. Larraza, T. Calvo-Correas, L. Martin, C. Derail, and A. Eceiza, "Enhancing the Mechanical Properties of 3D-Printed Waterborne Polyurethane-Urea and Cellulose Nanocrystal Scaffolds through Crosslinking," *Polymers (Basel)*, vol. 14, no. 22, Nov 18 2022, doi: 10.3390/polym14224999.
- [60] A. Bahadur, M. Shoaib, S. Iqbal, A. Saeed, M. S. u. Rahman, and P. A. Channar, "Regulating the anticancer drug release rate by controlling the composition of waterborne polyurethane," *Reactive and Functional Polymers*, vol. 131, pp. 134-141, 2018, doi: 10.1016/j.reactfunctpolym.2018.07.014.
- [61] S. M. Kamath *et al.*, "Fabrication of tri-layered electrospun polycaprolactone mats with improved sustained drug release profile," *Sci Rep*, vol. 10, no. 1, p. 18179, Oct 23 2020, doi: 10.1038/s41598-020-74885-1.
- [62] P. F. Costa, A. M. Puga, L. Diaz-Gomez, A. Concheiro, D. H. Busch, and C. Alvarez-Lorenzo, "Additive manufacturing of scaffolds with dexamethasone controlled release for enhanced bone regeneration," *Int J Pharm*, vol. 496, no. 2, pp. 541-50, Dec 30 2015, doi: 10.1016/j.ijpharm.2015.10.055.
- [63] J. Oh *et al.*, "Synthesis of Thermoplastic Polyurethanes Containing Bio-Based Polyester Polyol and Their Fiber Property," *Polymers (Basel)*, vol. 14, no. 10, May 16 2022, doi: 10.3390/polym14102033.
- [64] Z. K. Alobad, M. Albozahid, H. Z. Naji, H. S. Alraheem, and A. Saiani, "Influence of hard segments content on thermal, morphological and mechanical properties of homo and co-polyurethanes: a comparative study," *Archives of Materials Science and Engineering*, vol. 1, no. 109, pp. 5-16, 2021, doi: 10.5604/01.3001.0015.0510.
- [65] Y. Lu and R. C. Larock, "Soybean-Oil-Based Waterborne Polyurethane Dispersions: Effects of Polyol Functionality and Hard Segment Content on Properties," *Biomacromolecules*, vol. 9, no. 11, pp. 3332-3340, 2008/11/10 2008, doi: 10.1021/bm801030g.
- [66] B. Ranjbarfar, S. Taghvaei Ganjali, M. M. Alavi Nikje, and S. Moradi, "Synthesis, Characterization and Physicomechanical Properties of Novel Water-based Biodegradable Polyurethane Dispersion," *Russian Journal of Applied Chemistry*, vol. 91, no. 7, pp. 1198-1208, 2018, doi: 10.1134/s1070427218070200.

- [67] F. H. Zulkifli, F. S. Jahir Hussain, M. S. B. Abdull Rasad, and M. Mohd Yusoff, "In vitro degradation study of novel HEC/PVA/collagen nanofibrous scaffold for skin tissue engineering applications," *Polymer Degradation and Stability*, vol. 110, pp. 473-481, 2014, doi: 10.1016/j.polymdegradstab.2014.10.017.
- [68] R. Anand, N. Nimi, V. P. Sivadas, L. P. Merlin Rajesh Lal, and P. D. Nair, "Dual crosslinked pullulan-gelatin cryogel scaffold for chondrocyte-mediated cartilage repair: synthesis, characterization and in vitro evaluation," *Biomed Mater*, vol. 17, no. 1, Nov 11 2021, doi: 10.1088/1748-605X/ac338b.
- [69] A. Pryadko, M. A. Surmeneva, and R. A. Surmenev, "Review of Hybrid Materials Based on Polyhydroxyalkanoates for Tissue Engineering Applications," *Polymers (Basel)*, vol. 13, no. 11, May 26 2021, doi: 10.3390/polym13111738.
- [70] P. Haghighi and A. Shamloo, "Fabrication of a novel 3D scaffold for cartilage tissue repair: In-vitro and in-vivo study," *Mater Sci Eng C Mater Biol Appl*, vol. 128, p. 112285, Sep 2021, doi: 10.1016/j.msec.2021.112285.
- [71] K. C. Hung, C. S. Tseng, and S. H. Hsu, "Synthesis and 3D printing of biodegradable polyurethane elastomer by a water-based process for cartilage tissue engineering applications," *Adv Healthc Mater*, vol. 3, no. 10, pp. 1578-87, Oct 2014, doi: 10.1002/adhm.201400018.
- [72] S. F. Hashemi, M. Mehrabi, A. Ehterami, A. M. Gharravi, F. S. Bitaraf, and M. Salehi, "In-vitro and in-vivo studies of PLA / PCL / gelatin composite scaffold containing ascorbic acid for bone regeneration," *Journal of Drug Delivery Science and Technology*, vol. 61, 2021, doi: 10.1016/j.jddst.2020.102077.
- [73] T. Tayebi *et al.*, "Biofabrication of chitosan/chitosan nanoparticles/polycaprolactone transparent membrane for corneal endothelial tissue engineering," *Sci Rep*, vol. 11, no. 1, p. 7060, Mar 29 2021, doi: 10.1038/s41598-021-86340-w.
- [74] P. Si and B. Zhao, "Water-based polyurethanes for sustainable advanced manufacture," *The Canadian Journal of Chemical Engineering*, vol. 99, no. 9, pp. 1851-1869, 2021, doi: 10.1002/cjce.24049.
- [75] S. Kore, M. Theodore, and U. Vaidya, "Effect of the Segmental Structure of Thermoplastic Polyurethane (Hardness) on the Interfacial Adhesion of Textile-Grade Carbon Fiber Composites," *ACS Applied Polymer Materials*, vol. 3, no. 12, pp. 6138-6146, 2021, doi: 10.1021/acsapm.1c01001.
- [76] J. H. Bae *et al.*, "Synthesis and Characteristics of Eco-Friendly 3D Printing Material Based on Waterborne Polyurethane," *Polymers (Basel)*, vol. 13, no. 1, Dec 24 2020, doi: 10.3390/polym13010044.

- [77] N. Elmrbet and P. Siegkas, "Dimensional considerations on the mechanical properties of 3D printed polymer parts," *Polymer Testing*, vol. 90, 2020, doi: 10.1016/j.polymertesting.2020.106656.
- [78] J. Majko, M. Vasko, M. Handrik, and M. Saga, "Tensile Properties of Additively Manufactured Thermoplastic Composites Reinforced with Chopped Carbon Fibre," *Materials (Basel)*, vol. 15, no. 12, Jun 14 2022, doi: 10.3390/ma15124224.
- [79] M. Qamar Tanveer, G. Mishra, S. Mishra, and R. Sharma, "Effect of infill pattern and infill density on mechanical behaviour of FDM 3D printed Parts- a current review," *Materials Today: Proceedings*, vol. 62, pp. 100-108, 2022, doi: 10.1016/j.matpr.2022.02.310.
- [80] R. Srinivasan, K. Nirmal Kumar, A. Jenish Ibrahim, K. V. Anandu, and R. Gurudhevan, "Impact of fused deposition process parameter (infill pattern) on the strength of PETG part," *Materials Today: Proceedings*, vol. 27, pp. 1801-1805, 2020, doi: 10.1016/j.matpr.2020.03.777.
- [81] M. Lalegani Dezaki, M. K. A. M. Ariffin, A. Serjouei, A. Zolfagharian, S. Hatami, and M. Bodaghi, "Influence of Infill Patterns Generated by CAD and FDM 3D Printer on Surface Roughness and Tensile Strength Properties," *Applied Sciences*, vol. 11, no. 16, 2021, doi: 10.3390/app11167272.
- [82] A. Chadha, M. I. Ul Haq, A. Raina, R. R. Singh, N. B. Penumarti, and M. S. Bishnoi, "Effect of fused deposition modelling process parameters on mechanical properties of 3D printed parts," *World Journal of Engineering*, vol. 16, no. 4, pp. 550-559, 2019, doi: 10.1108/wje-09-2018-0329.
- [83] I. Karakurt, A. Aydogdu, S. Cikrikci, J. Orozco, and L. Lin, "Stereolithography (SLA) 3D printing of ascorbic acid loaded hydrogels: A controlled release study," *Int J Pharm*, vol. 584, p. 119428, Jun 30 2020, doi: 10.1016/j.ijpharm.2020.119428.
- [84] E. Dalton, Q. Chai, M. W. Shaw, T. J. McKenzie, E. S. Mullins, and N. Ayres, "Hydrogel-coated polyurethane/urea shape memory polymer foams," *Journal of Polymer Science Part A: Polymer Chemistry*, vol. 57, no. 13, pp. 1389-1395, 2019, doi: 10.1002/pola.29398.
- [85] H. Baniyadi, Z. Madani, R. Ajdary, O. J. Rojas, and J. Seppala, "Ascorbic acid-loaded polyvinyl alcohol/cellulose nanofibril hydrogels as precursors for 3D printed materials," *Mater Sci Eng C Mater Biol Appl*, vol. 130, p. 112424, Nov 2021, doi: 10.1016/j.msec.2021.112424.
- [86] X. Yin *et al.*, "Chemical Stability of Ascorbic Acid Integrated into Commercial Products: A Review on Bioactivity and Delivery Technology," *Antioxidants (Basel)*, vol. 11, no. 1, Jan 13 2022, doi: 10.3390/antiox11010153.

- [87] S. Mirzaeei, F. Moghadam, K. Asare-Addo, and A. Nokhodchi, "Design of a nanofibrous guided tissue regeneration carrier as a potential drug delivery system for tetracycline hydrochloride in the management of periodontitis," *Journal of Drug Delivery Science and Technology*, vol. 75, 2022, doi: 10.1016/j.jddst.2022.103722.
- [88] A. Korelidou *et al.*, "3D-printed reservoir-type implants containing poly(lactic acid)/poly(caprolactone) porous membranes for sustained drug delivery," *Biomater Adv*, vol. 139, p. 213024, Aug 2022, doi: 10.1016/j.bioadv.2022.213024.
- [89] E. Tamjid, M. Bohlouli, S. Mohammadi, H. Alipour, and M. Nikkhah, "Sustainable drug release from highly porous and architecturally engineered composite scaffolds prepared by 3D printing," *J Biomed Mater Res A*, vol. 108, no. 6, pp. 1426-1438, Jun 2020, doi: 10.1002/jbm.a.36914.
- [90] G. R. da Silva, A. da Silva-Cunha, F. Behar-Cohen, E. Ayres, and R. L. Oréfice, "Biodegradable polyurethane nanocomposites containing dexamethasone for ocular route," *Materials Science and Engineering: C*, vol. 31, no. 2, pp. 414-422, 2011, doi: 10.1016/j.msec.2010.10.019.